

Polytechnic Institute of New York

AFOSR-TR- 81 - 0155

Aerodynamics Laboratories

Department of Mechanical

&

Aerospace Engineering



HYPERSONIC AND OTHER VISCOUS INTERACTIONS

Robert J. Cresci

LEVEL II

APPENDIX A

THREE-DIMENSIONAL VISCOUS INTERACTIONS

Stanley G. Rubin

S DTIC ELECTE D
MAR 0 2 1981
E

FINAL REPORT

November 1, 1977 - September 30, 1980

December 1980

POLY M/AE Report 80-32

81 2 27 076

Approved for public release;
distribution unlimited.

AD A 095817

DUPLICATE COPY

↓
internal flow problems. In this area, the development of numerical techniques and analytical tools is of primary significance although the application of these methods to practical problems of interest has also been accomplished. *M*

FINAL REPORT

on

Contract No. **DF**49620-78-C-0020, Project No. 2307-AI

for the period

November 1, 1977 - September 30, 1980

HYPERSONIC AND OTHER VISCOUS INTERACTIONS

Robert J. Cresci
Polytechnic Institute of New York
Aerodynamics Laboratories

APPENDIX A

THREE-DIMENSIONAL VISCOUS INTERACTIONS

Stanley G. Rubin
Polytechnic Institute of New York
Aerodynamics Laboratories

December 1980

Accession For	
NTIS GRA&I	<input checked="" type="checkbox"/>
DTIC TAB	<input type="checkbox"/>
Unannounced	<input type="checkbox"/>
Justification	
By _____	
Distribution/	
Availability Codes	
Dist	Avail and/or Special
A	

AIR FORCE OFFICE OF SCIENTIFIC RESEARCH (AFSC)
REPORT NUMBER 80-32
This report has been reviewed and is
approved for release under E.O. 11652 (7b).
Distribution is unlimited.
A. D. BLUM
Technical Information Officer

POLY M/AE Report No. 80-32

SUMMARY

The studies performed under this contract fall into two major categories:

- (i) A study of transpiration cooling of typical hypersonic re-entry configurations with a primary emphasis on experimental data acquisition, although some limited analytical and numerical support studies have been undertaken. The experiments have been conducted in the hypersonic flow region, under zero and non-zero angle of attack conditions, and covering the range in Reynolds numbers required to obtain laminar, transitional, and turbulent data.
- (ii) Numerical and analytical studies of viscous and interacting viscous-inviscid flows with application to 3D boundary layers, wing-body configurations, and internal flow problems. In this area, the development of numerical techniques and analytical tools is of primary significance although the application of these methods to practical problems of interest has also been accomplished.

The principal investigators on this contract for the period November 1977 through August 1979 were Prof. M. H. Bloom, Prof. R. J. Cresci, and Prof. S. G. Rubin. For the remainder of the contract period, Prof. M. H. Bloom and Prof. R. J. Cresci served as principal investigators since Prof. S. G. Rubin left the Polytechnic Institute.

The technical area summarized in (i) above is described in the following section; the numerical studies summarized in (ii) have already been issued as a Final Report and, therefore, will be included here as an Appendix.

Table of Contents

Summary	i
Film Cooling Studies	1
(1) Transition location determination	2
(2) Boundary Layer Relaminarization	3
(3) Numerical Analysis of Laminar Boundary Layers	4
(4) Angle of Attack Tests	5
(5) New Data Acquisition System	7
(6) Liquid Film Cooling	8
References	13
Figures (1) through (22)	
Appendix A - Three Dimensional Viscous Interactions by S. G. Rubin	A-1
(1) Spline Deferred-Corrector Interpolation	A-2
(2) Coupled Calculation Procedure	A-4
(3) Parabolized Navier-Stokes Equations	A-6
(4) Internal Flows	A-8
(5) Wing-Body Secondary Flow Interaction	A-10
Figures A1 through A 11	

FILM COOLING STUDIES

With the renewed interest in highly maneuverable vehicles, capable of relatively long duration flights in the atmosphere, at supersonic and hypersonic speeds, active surface cooling systems have regained significance as technological problems of practical interest. Although ablative or other passive cooling systems have proven successful for reentry vehicles, there are difficulties associated with their use in the current flight conditions of interest. One of the simplest active systems proposed is to inject a liquid, or a gas, through a porous surface in regions of high aerodynamic heating and thereby cool the surface locally. Some additional "persistence" of cooling effect is usually realized downstream of the porous region. This effect may be used to optimize the coolant mass flow required to maintain the structural integrity of the surface. However, the injected coolant tends to thicken the boundary layer and thereby initiate transition of the boundary layer from laminar to turbulent prematurely. As a result, under certain circumstances addition of a coolant may actually increase the total aerodynamic heating to the vehicle surface, rather than cool it as desired.

A primary objective of this program is to evaluate the phenomena of boundary layer transition in an attempt to arrive at the ability to predict transition onset due to film cooling. This is essential if such active cooling systems are to be designed and implemented effectively under a wide variety of flight conditions. The current program was initiated several years ago, utilizing both liquid (water) and gaseous (nitrogen) coolants.

The experimental and corresponding analytical program involved with gaseous film cooling was conducted at a Mach number of 8.0 and over a range in free stream Reynolds numbers varying from fully laminar flow to transitional and turbulent flow. The model used in these tests corresponds to a slender cone (10° half angle) with a spherical nose tip. A porous section of 60° total included angle is inserted in the model nose for mass transfer purposes. With this configuration the boundary layer is completely laminar over the entire surface even at the higher test Reynolds numbers when there is zero mass injection. With injection, however, the nature of the boundary layer changes to transitional and/or turbulent flow depending on the surface location, mass transfer rate, and free stream Reynolds number. Some of the specific effects relating to this behavior are described below.

(1) Transition location determination

Usually, one can determine boundary layer transition from surface heat transfer measurements, however, when transpiration cooling is present, the transition location is obscured. Since the data at a specific surface location exhibits a monotonically decreasing trend with increasing coolant flow rate, the transition location is difficult to determine accurately under certain circumstances. If a theoretical analysis based on laminar boundary layer behavior is available, the transition location usually becomes more apparent cf. figure (1). While this approach has been used successfully, the numerical counterpart for non-zero angle of attack conditions, or other more complicated configurations is not currently available. Moreover, under cer-

tain conditions (such as the location $\bar{S} = 2.95$ in figure (1)) the deviation of the data from the laminar theory is so gradual that the transition location is difficult to detect accurately.

As a result, an attempt was made to use surface thin film probes to determine the transition location. The primary parameter of interest which was capable of being correlated with the transition location was the RMS output of the thin film gauge of reference (1). Examination of the mean voltage or the spectral distribution of the fluctuating voltage produced by the constant temperature anemometer provided no information in this regard. Test data indicated that the RMS output of the surface film gauges may be used to determine transitional behavior even when active cooling is present. Examination of figure (2) clearly shows the transition location even under otherwise difficult conditions. Moreover, the thin film technique provides a means for determining the transition location without resorting to a theoretical analysis of the flow field. Configurations and flow fields may now be investigated for which no theoretical analysis is available. The only drawback to this technique is that a large number of tests are required to determine the specific transitional behavior at one surface location on the test model.

(2) Boundary layer relaminarization

The general behavior of a transpiration cooled slender cone was described in detail in reference (2) with respect to the transitional behavior of the boundary layer. One of the more surprising results that was obtained from this study was that transitional flow was observed close to the injection region, followed by a region of laminar flow which in turn was followed by another region

of transitional boundary layer of figure (3). This behavior occurred only at certain Reynolds numbers and implied a local relaminarization of the boundary layer. To verify this effect, measurements were made with thin film surface gauges and the results of this study are described in reference (3). Figure (4) shows the variation of mass transfer required to initiate transition, with surface location. At any specified location, the boundary layer is laminar until the mass transfer rate exceeds a particular value ($N_{c_{TR}}$). For larger values of mass injection, the boundary layer becomes transitional. In order to perceive the relaminarization phenomena, one must consider the distribution along the surface at a particular mass transfer rate. For the conditions of figure (4), a mass transfer rate corresponding to $N_c \approx 8$ will not alter the laminar behavior of the boundary layer over the entire surface.

If the mass injection is increased to $N_c \approx 16$, however, it is evident that a region of laminar flow is followed by a transitional regime, which is the expected behavior. Further downstream, however, the flow again becomes laminar as seen by the increase of $N_{c_{TR}}$.

(3) Numerical analysis of laminar boundary layers

The numerical analysis of a film cooled, blunted cone at angle of attack using the thin shock layer approximation has been developed and programmed for solution on the IBM 360-65 computer. The flow over the porous injection region has been solved and will provide the initial conditions for the non-zero angle of attack program, cf. reference (4). Although the porous region has been analyzed previously by a boundary layer approach for small injection,

and by matching two inviscid rotational layers for large mass transfer, the present approach is the only one available that provides the complete viscous and inviscid layer characteristics from the body surface to the bow shock wave. A typical result showing the fluid velocity, temperature, and density is shown in figure (5). The two-layer inviscid behavior is evident, although the present analysis also predicts the shear layer separating the free stream and the injected coolant fluids. Another result that can be compared with experiments is the shock stand-off distance. This is shown in figure (6) and the agreement with the data of Ref. (5) is seen to be reasonably good.

The interface distance is also shown in figure (7) and compared with the location predicted by the inviscid analysis of Ref. (5). The present method shows a band, for each coolant flow rate, where the band defines the edges of the viscous shear layer. The agreement here is seen to be excellent. The nature of this shear layer is important, since it has been suggested that the transitional effects observed on the downstream conical surface originate in the shear layer, due to the very large gradients occurring therein. This phenomena has yet to be investigated.

(4) Angle of attack tests

The mass transfer model has been tested at a variety of Reynolds numbers, coolant mass flow rates, and angles of attack of 2° , 6° , 10° and 14° . An overall data plot of heat transfer vs. surface location is shown in figure (8) for small angles of attack ($\alpha = 2^\circ$). Here, the flow characteristics deviate only slightly from the symmetric, $\alpha = 0$, test condition. The cooling effectiveness extends roughly nine nose radii downstream, although even at

that distance some transitional behavior is evident since the higher coolant flow rate increases the surface heat transfer (rather than decreasing it as desired). If the angle of attack is increased to 10° (the half-cone angle) the region of coolant effectiveness is seen in figure (9) to decrease to about four nose radii downstream. The region of interest here is on the windward surface since the leeward surface experiences an extremely low heat transfer rate even without mass transfer cooling. Despite the loss in coolant effectiveness at the larger angles of attack, this coolant system is still reasonably good since it does reduce the stagnation region heat transfer to zero on the porous region (note the temperature distribution given in figure (5)). With no active cooling system in operation, the stagnation heat rates are an order of magnitude larger than those occurring on the windward plane.

In order to examine the angle of attack behavior in more detail, figure (10) presents the surface heat transfer on the windward ray for a location close to the end of the porous region ($\bar{s} = 1.36$). Although the coolant reduces the heat transfer at all of the test angles of attack, the coolant effectiveness is seen to decrease rapidly as α increases. On the leeward ray, cf. figure (11), the coolant effectiveness is seen to be enhanced as the angle of attack increases. This behavior is the result of two separate effects. First, since the porous injection region is symmetric about the cone body axis, when the cone is at an angle of attack the effective length of the injection region on the windward surface becomes less than on the leeward surface due to the windward movement of the stagnation point. The second effect is due to the cross flow of boundary layer fluid from the windward toward the lee-

ward plane. This also reduces the coolant mass in the windward plane boundary layer region thus reducing its effectiveness.

As the downstream distance increases, the coolant effectiveness deteriorates until, at a location of eight and a half nose radii downstream, the effect of mass injection is no longer apparent (on the windward plane); this may be observed in figure (12). It is not yet evident whether this effect is entirely due to the reduced coolant effectiveness, or whether boundary layer transition has eliminated any residual coolant effect. It is anticipated that the latter will be true, however, this can only be definitely ascertained by using the thin film technique.

(5) New data acquisition system

Since the film cooling program at the Polytechnic is heavily, although not exclusively, oriented toward experiments, a significant improvement in the wind tunnel data acquisition system which occurred during the current period is an important factor in enhancing the experimental capabilities of the Aerodynamics Laboratories. A Honeywell Model 101 tape recording system has been purchased and interfaced with a DEC PDP 1134 minicomputer both of which are located in the wind tunnel facility. Following the data acquisition on the magnetic tape from a wind tunnel test, it is reproduced and transformed into digital form by the PDP 1134 A/D convertors. Some software for data analysis and processing has been developed for the type of information normally obtained from the wind tunnel. The data is then plotted on a Techtronix CRT-4006 terminal, and if desired hard copies can be obtained from a Tektronix 4631 hard copy unit. A typical result is shown in figure (13) which presents the temperature distribution as a func-

tion of time for a specific model location ($\bar{s} = 1.36$). A curve fit is applied to the data which is then reduced to produce the Nusselt number distribution with time as shown in figure (14).

(6) Liquid film cooling

A program in liquid film cooling was initiated several years ago and it was found that the liquid film persistence could not be predicted on the basis of aerodynamic heating or film instabilities. This led to a program in diagnostics of two-phase flow systems in a supersonic environment. The detailed diagnostics of such flow systems has, in the past, been extremely difficult to achieve without significant disturbances to the flow system under investigation. Invariably, the techniques utilized have altered either the flow conditions or the composition between the sampling location and the measuring station. Optical techniques do not have this inherent difficulty and, in particular, Raman spectroscopy has provided this non-intrusive capability in static systems for many years.

A summary report on the results obtained with the previously available laser diagnostic system has been presented in reference (6). This summarized the static chamber evaluation of the system and provided accurate results in addition to further insight into the application of the system to moving flow systems.

Some problems became evident in the application of the available laser system to actual test conditions in a hypersonic tunnel. For example, the thin boundary layer, and the close proximity of the laser beam to the wall of the model, cause considerable difficulties due to the inability to focus the original dye laser to a fine beam width. Regarding the Raman scattering properties,

the low scattering cross-section and the frequency shift, caused by the water and water vapor, into the infrared regime made the detection of the scattered photons difficult due to the very low quantum efficiency of the available photomultiplier tubes in the near infrared frequency range. With a ruby laser of 6943\AA wavelength radiation, the Raman Stokes wavelength would be 7840\AA and 9303.6\AA for water vapor and water droplets, respectively, since the vibrational frequency for liquid water is 1648cm^{-1} , and for water vapor is 3654.5cm^{-1} .

To alleviate this problem and provide maximum resolution in the boundary layer with the optimum signal-to-noise ratio, the Coherent anti-Stokes Raman scattering technique (CARS) was suggested to measure the constituents in the boundary layer.

Since the vibrational frequency shift for liquid water as indicated above, is 1648cm^{-1} and that of water vapor is 3654.5cm^{-1} , the anti-Stokes wavelengths with the primary radiation of 5145\AA from an Argon ion laser would be 4742.8\AA and 4330\AA , respectively. This places the scattered signal in the range of very high quantum efficiency of available photomultiplier tubes and, in addition, the resulting narrow coherent beam permits excellent resolution and detection. As is well-known, the CARS system is essentially a non-linear system resulting from a combination of an incident wavelength with the corresponding Stokes wavelength ω_s to generate an anti-Stokes wavelength ω_{as} such that $\omega_{as} = 2\omega_p - \omega_s$. The power $P(\omega_{as})$ is proportional to:

$$P(\omega_p)^2 \times P(\omega_s)$$

The Stokes wave, ω_s , can be generated by stimulated Raman emission using the incident beam, ω_p , which could be a Ruby laser; however,

for each specie to be measured its generated Stokes line must be of sufficient intensity. This is generally accomplished by using a special cell where a sample of the gas under investigation must be kept at high pressure, and illuminated with an incident laser beam ω_p of sufficient intensity to facilitate the stimulated emission. In the case of water vapor this becomes extremely difficult since the vapor will not remain in equilibrium at high pressures. Another method which can be used to achieve the generation of the CARS effect is to use an externally generated ω_s and combine it at the point of diagnosis with ω_p . This can be done using a tunable dye laser, which could generate most of the Stokes lines of interest. In particular, for the two-phase water system of interest here, the Stokes line using an Argon ion laser of 5145Å primary light is 5621.7Å and 6336.4Å for liquid and vapor water, respectively. This laser equipment was not available in the Aerodynamics Laboratories and had to be purchased, following a detailed design of the available diagnostic apparatus.

The major pieces of equipment consisting of two Argon-ion C-W lasers (Control Laser Corp.) and a tunable dye laser (Coherent Radiation Model 590) have been purchased. Up to this point progress was according to schedule. A schematic diagram of a c-w CARS system is shown in Fig. (15). However since the delivery of this equipment a number of problems arose. Without entering into the specifics, it turned out that the continuous wave system based on the Argon-ion lasers had to be abandoned, basically due to the unreliability of the lasers supplied to us by the Control Laser Corporation of Orlando, Florida.

A new laser system which became available to us has therefore

been utilized for the development of a reliable CARS system to measure water vapour and water liquid. Preliminary tests indicate a very high sensitivity of the system to water vapour. As an example, the system is capable of detecting the content of water vapor of room air. This is shown in Fig. (16) which is a photographic record taken from the multichannel spectrum analyzer. The amplitude shown represents about 68000 counts. Fig. (17) shows the amplitude obtained from water vapor found above boiling water at atmospheric conditions. The amplitude here represents approximately 440000 counts. The number of scans in each case as seen in the pictures correspond to 1250. These data points are only of a preliminary nature. They were obtained using the coaxial CARS system as shown in Fig. (18a). In Fig. (19) the normalized radial profile of water vapor of a steam jet is shown.

At this point the system as shown in Fig. (18a) is capable of measuring liquid water. The signals as shown in Fig. (20) are of a fixed amount of water in a cylindrical vessel, as shown in Fig. (21). It is evident that at this point the colinear CARS system as shown in Fig. (18a) is performing quite well. However as discussed in the progress reports, the spatial resolution of this system is not very good. This feature of the coaxial system has been confirmed experimentally and is shown in Fig. (22). As seen in this figure, the CARS emission from the section of the focussed beams, one cm to either side of the focal point (plane), is about 20% compared to the emission from the focal point. While the resolution as shown is characteristic of the system as shown in Fig. (18a), the Box CARS system of Fig. (18b) has a pointwise resolution. This system is being tested presently. No experimen-

tal results are available at this time for the Box CARS system.

References

1. Owen, F.K.: Transition Experiments on a Flat Plate at Subsonic and Supersonic Speeds. AIAA J., pp. 518-523, March 1970.
2. Starkenberg, J. and Cresci, R.J.: Boundary Layer Transition on a Film Cooled Slender Cone. AIAA J., Vol. 14, No. 4, April 1976.
3. Plostins, P. and Cresci, R.J.: Boundary Layer Transition Detection on Film Cooled Bodies. Poly Report RD-249.
4. Plostin, P. and Rubin, S. G.: The Axisymmetric Stagnation Region Thin Shock Layer for Large Rates of Injection. POLY M/AE Report No. 80-24. September 1980.
5. Cresci, R.J. and Libby, P.A.: The Downstream Influence of Mass Transfer at the Nose of a Slender Cone. Pibal Report No. 634, WADD TR 60-892, AD 257 807, May 1961; also J. Aero. Sci., 29, 7, pp. 815-826, July 1962; also Authors' Reply to Comments on the Shock Stand-Off Distance with Stagnation-Point Mass Transfer by Marcel Vinokur. AIAA J., 1, 7, pp. 1712-1713, July 1963.
6. Lederman, S.: Development in Laser Based Diagnostic Techniques. POLY M/AE Report No. 79-23. Presented at the 12th International Shock Tube Symposium held July 16-20, 1979 at Hebrew University, Jerusalem, Israel.
7. Rubin, S.G., Khosla, P.K.: Turbulent Boundary Layers With and Without Mass Injection. Computers and Fluids, 5, 4, pp. 241-259, December 1977.

8. Rubin, S.G. and Khosla, P.K.: An Integral Spline Method For Boundary Layer Equations. Computers and Fluids, 7, 1, pp. 75-78, March 1978.
9. Rubin, S.G. and Khosla, P.K.: A Simplified Spline Solution Procedure. Proceedings of the Sixth International Conference on Numerical Methods in Fluid Dynamics, Tbilisi, Russia June 20-25, 1978.
10. Rubin, S.G. and Khosla, P.K.: Navier-Stokes Calculations with a Coupled Strongly Implicit Method, Part I: Finite-Difference Solutions. AIAA Paper No. 79-0011, AIAA 17th Aerospace Sciences Meetings, January 15-17, 1979, New Orleans, La.
11. Rubin, S.G. and Khosla, P.K.: Navier-Stokes Calculations With a Coupled Strongly Implicit Method, Part 2: Spline Deferred-Corrector Solutions. To be presented at the IUTAM Symposium on Approximation Methods for Navier-Stokes Problems, Paderborn, West Germany, September 9-15, 1979.
12. Khosla, P.K. and Rubin, S.G.: A Fast Iterative Algorithm for Multi-Dimensional Flow Problems. Presented at the Symposium on Computers in Aerodynamics, Polytechnic Institute of New York, June 4-5, 1979.
13. Davis, R.T. and Rubin, S.G.: Non-Navier-Stokes Viscous Flow Computations. Presented at the Symposium on Computers in Aerodynamics, Polytechnic Institute of New York, June 4-5, 1979, to appear Computers and Fluids.
14. Lin, T.C. and Rubin, S.G.: A Numerical Model for Supersonic Viscous Flow Over a Reentry Vehicle. AIAA paper No. 79-0205, AIAA 17th Aerospace Sciences Meeting, January 15-17, 1979, New Orleans, La.

15. Ghia, U., Ghia, K.N., Rubin, S.G. and Khosla, P.K.: Study of Incompressible Flow Separation Using Primitive Variables. Presented at the Symposium on Computers in Aerodynamics, Polytechnic Institute of New York, June 4-5, 1979.
16. Rubin, S.G. and Lyons, J.M.: Boundary Layer Induced Secondary Flows Due to Wing-Body Interference. AIAA paper No. 79-0140, AIAA 17th Aerospace Sciences Meeting, January 15-17, 1979, New Orleans, La., to appear AIAA Journal.

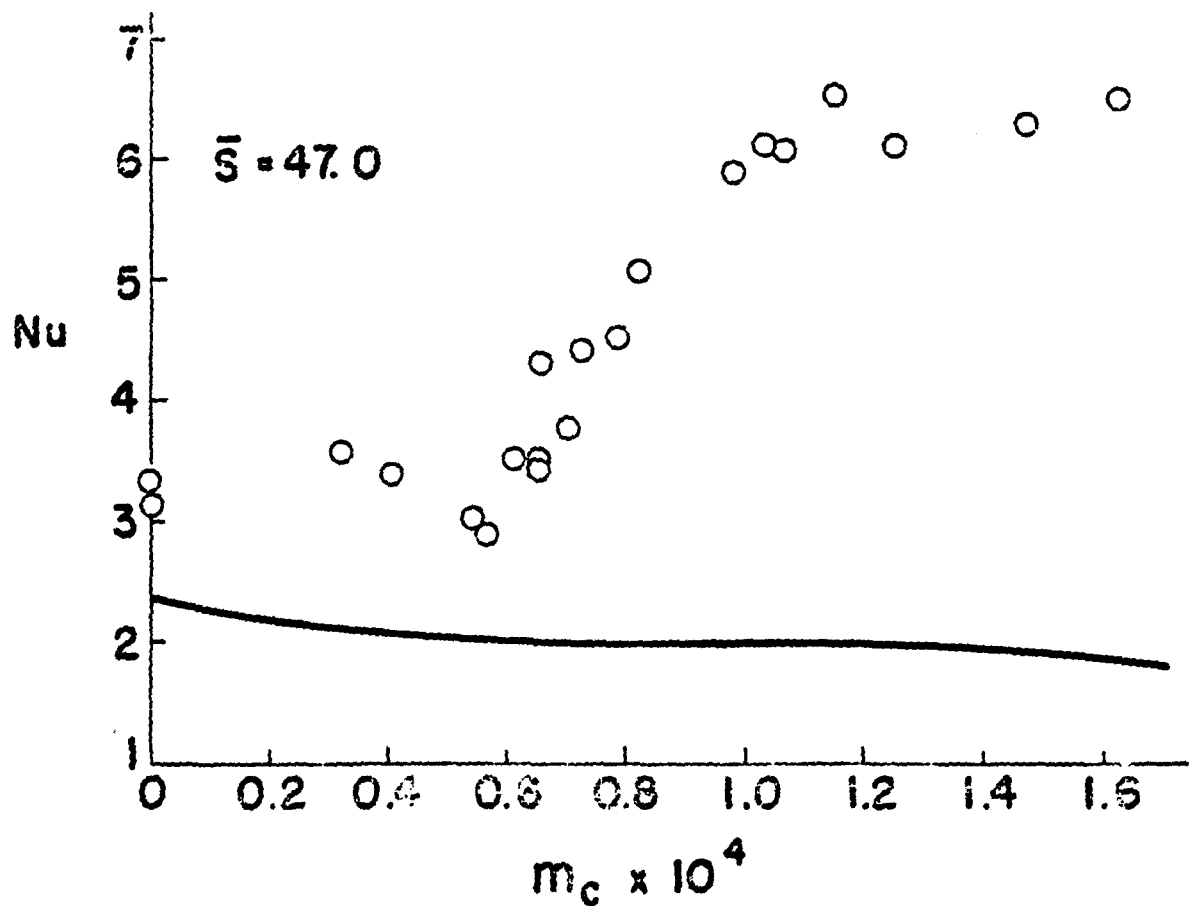
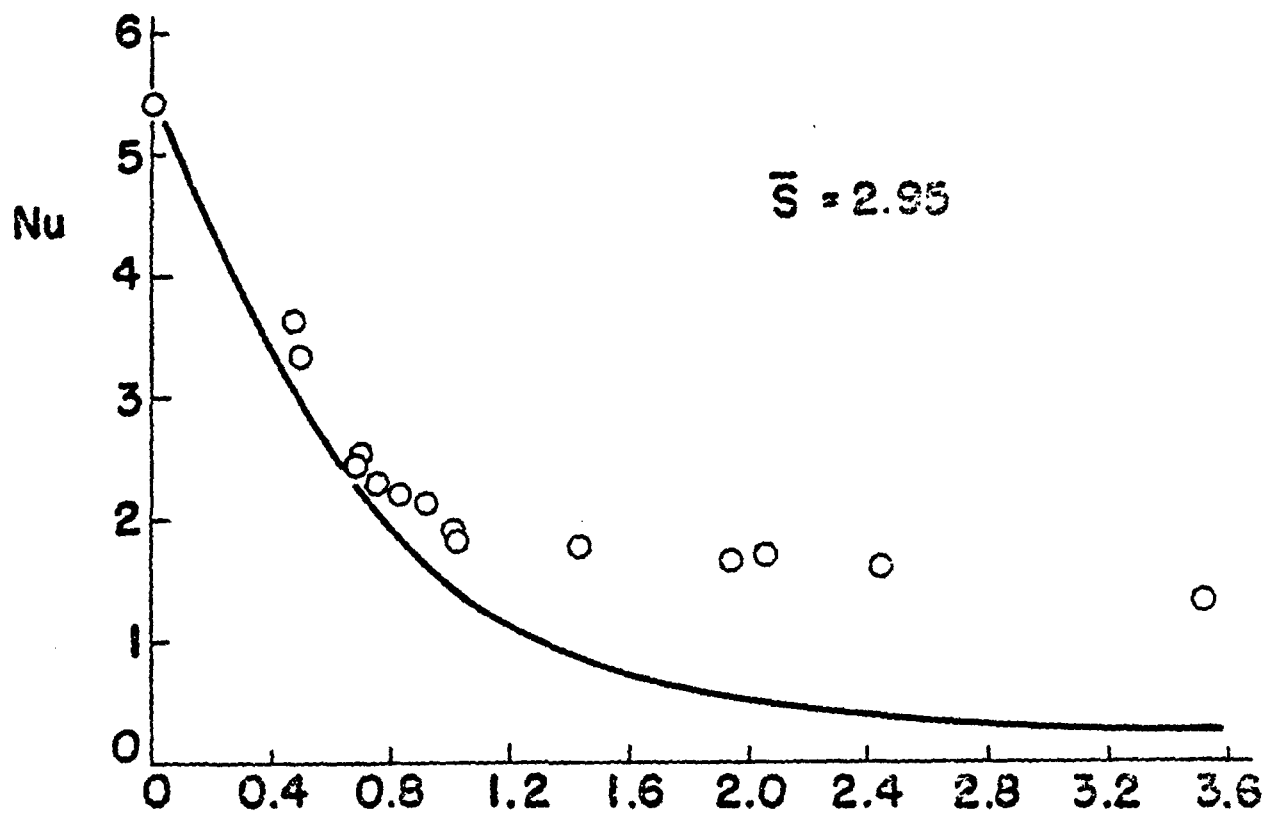


FIG. 1 COMPARISON OF HEAT TRANSFER DATA WITH LAMINAR THEORY

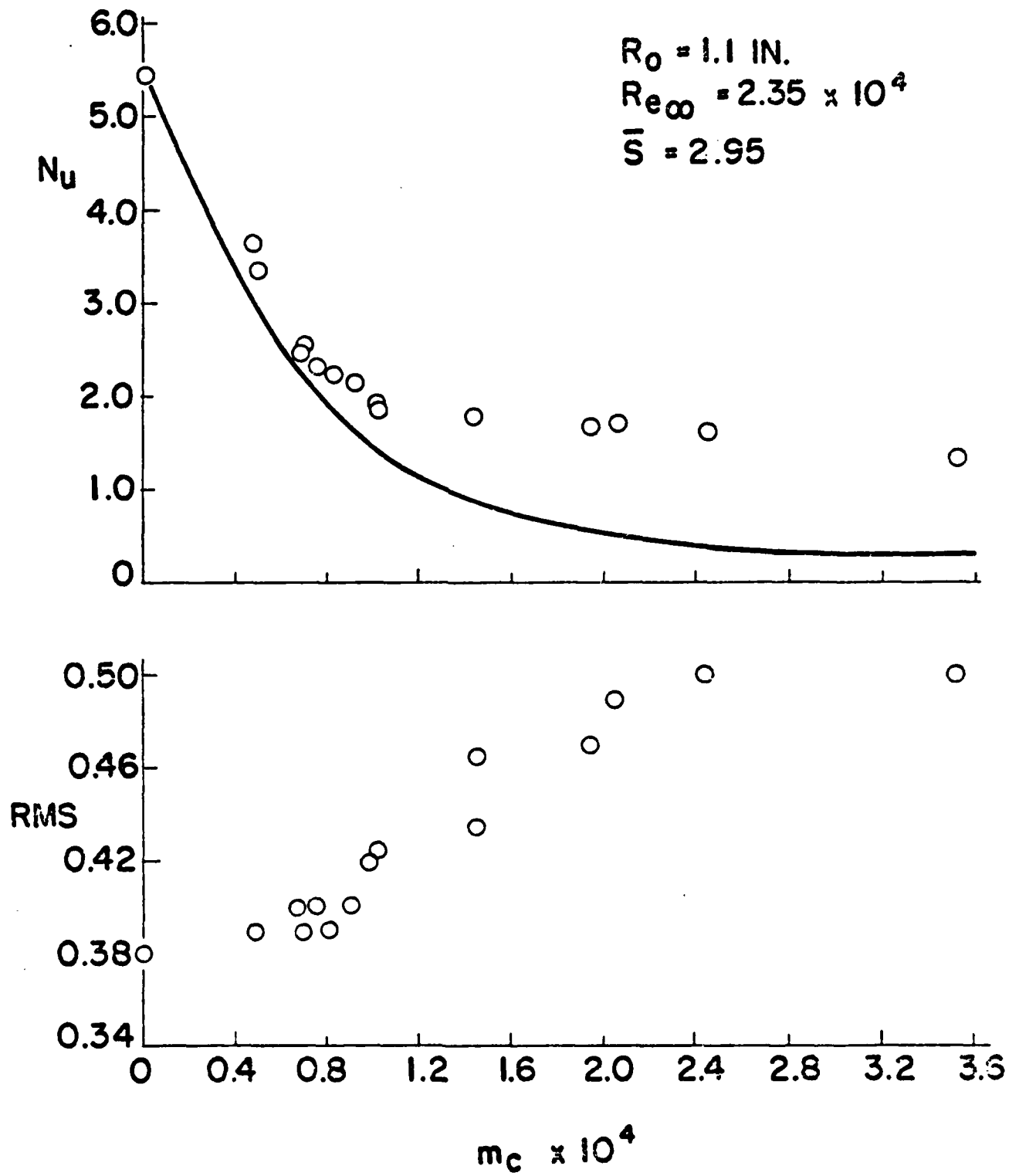


FIG. 2 COMPARISON OF SURFACE HEAT TRANSFER
 DATA AND RMS DATA

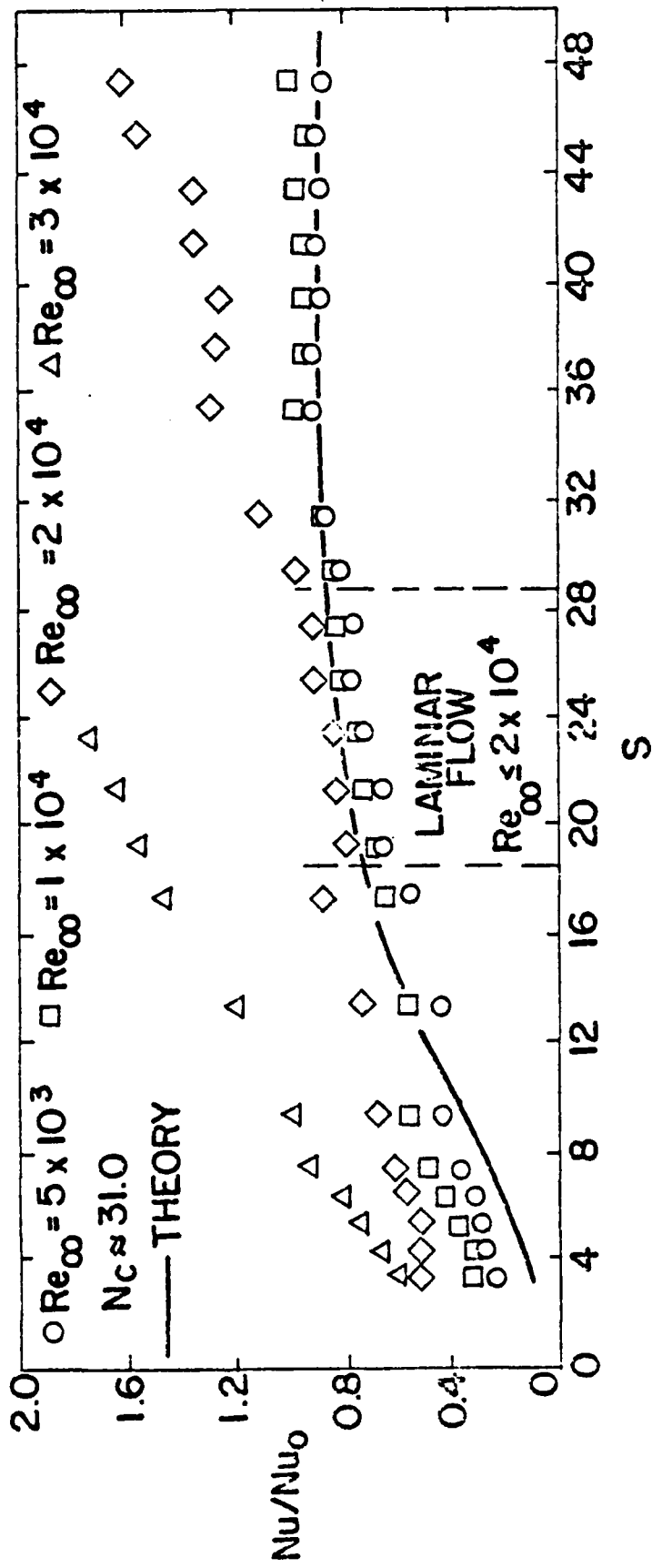


FIG. 3 HEAT TRANSFER VS SURFACE DISTANCE ($\alpha=0$)

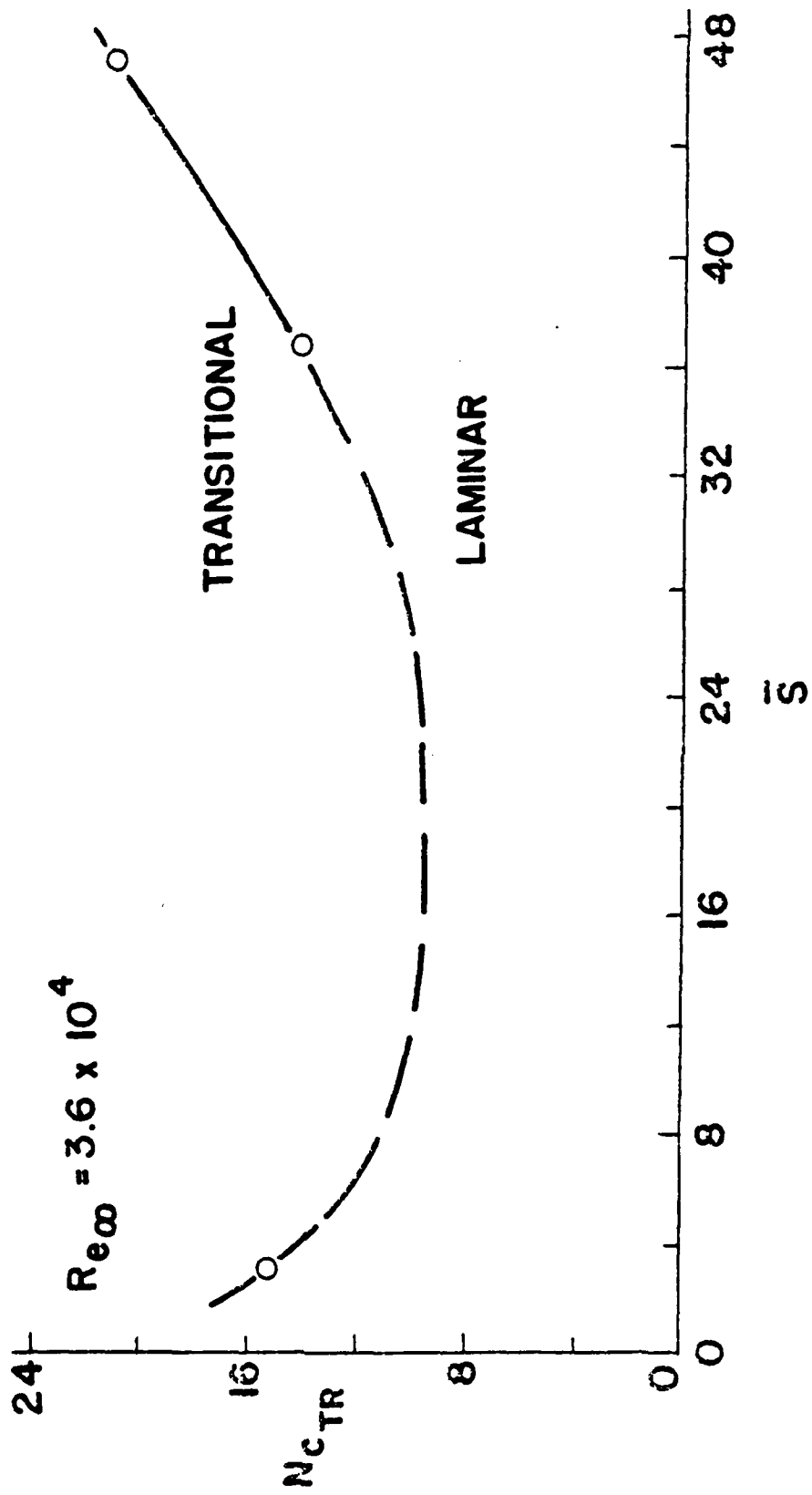
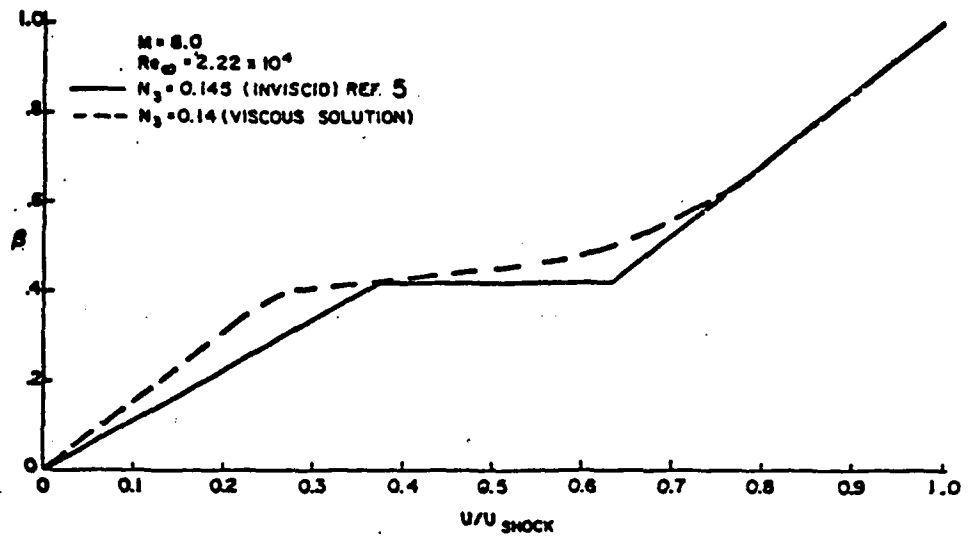
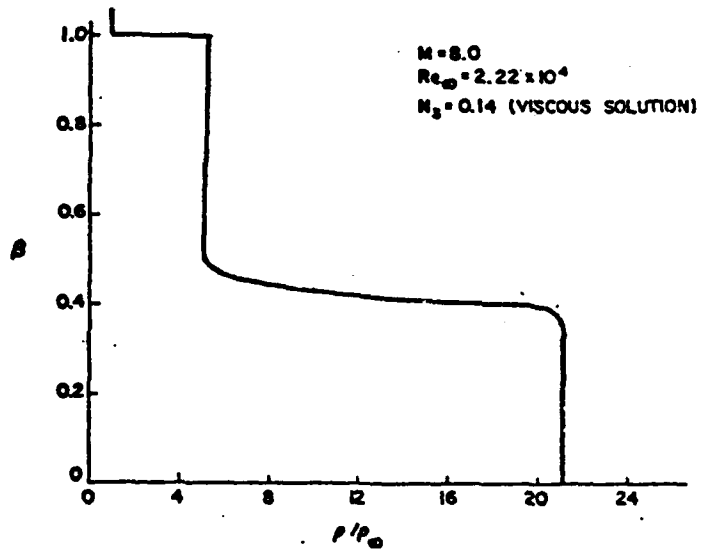


FIG. 4 RELAMINARIZATION EFFECT OF MASS TRANSFER



STAGNATION REGION - VELOCITY PROFILE



STAGNATION REGION - DENSITY PROFILE

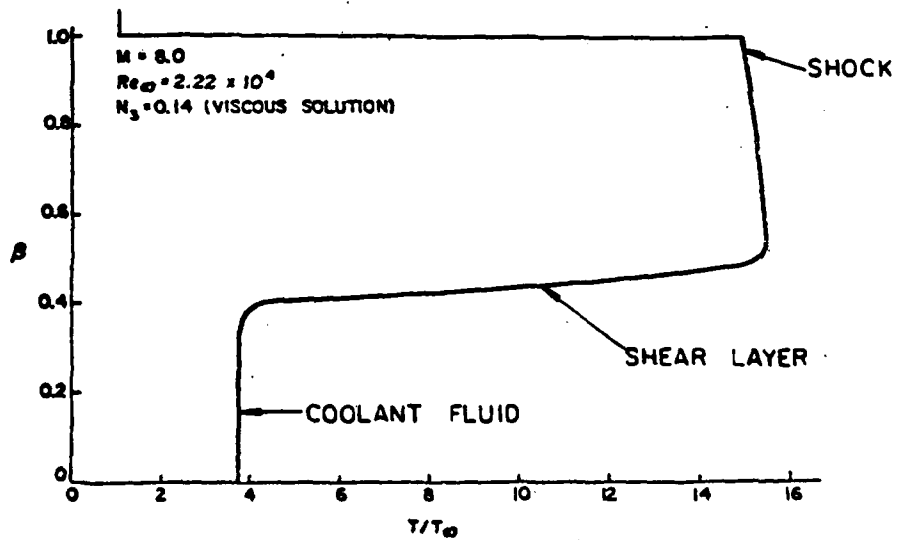


FIG. 5 STAGNATION REGION - TEMPERATURE PROFILE

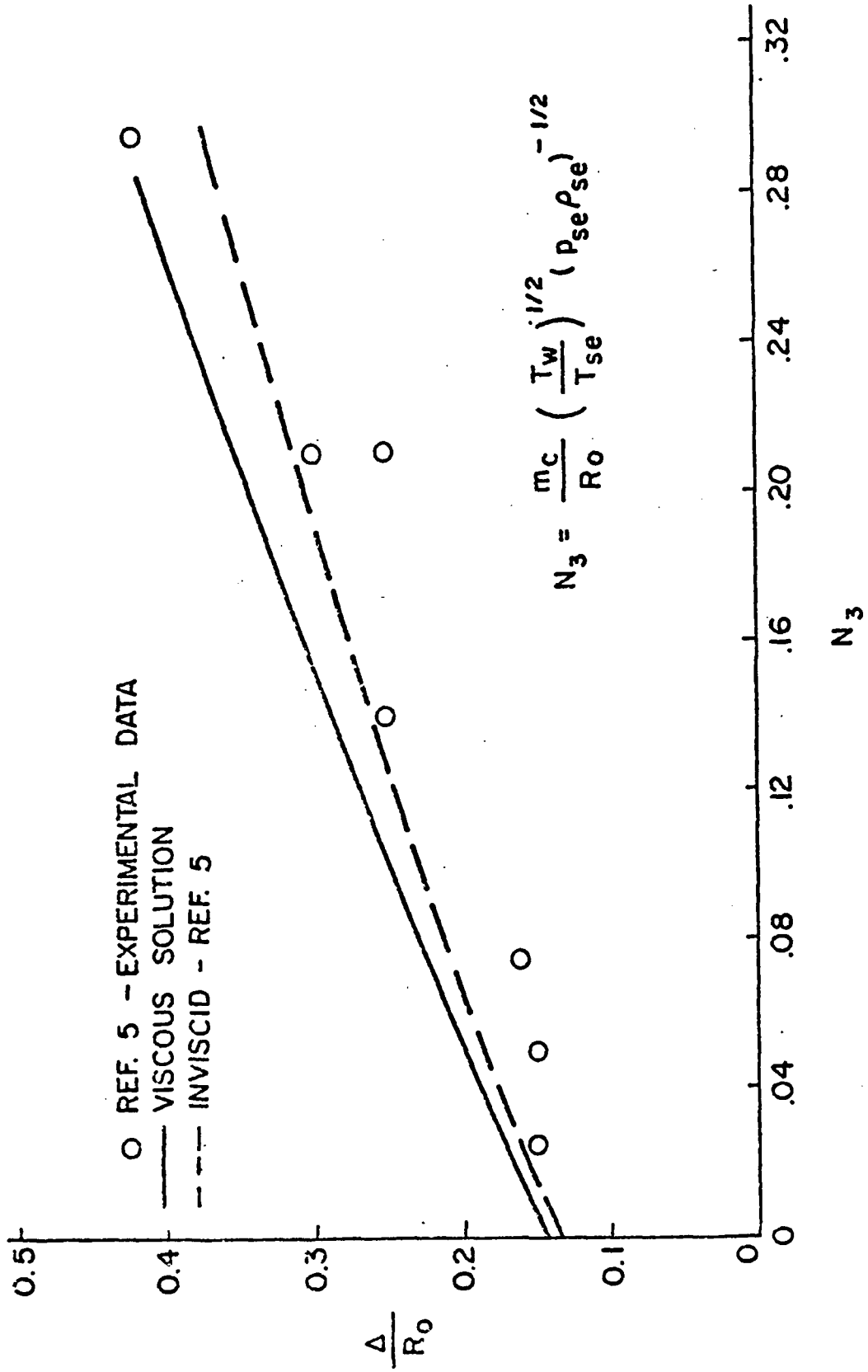


FIG. 6 STANDOFF DISTANCE VS INJECTION PARAMETER

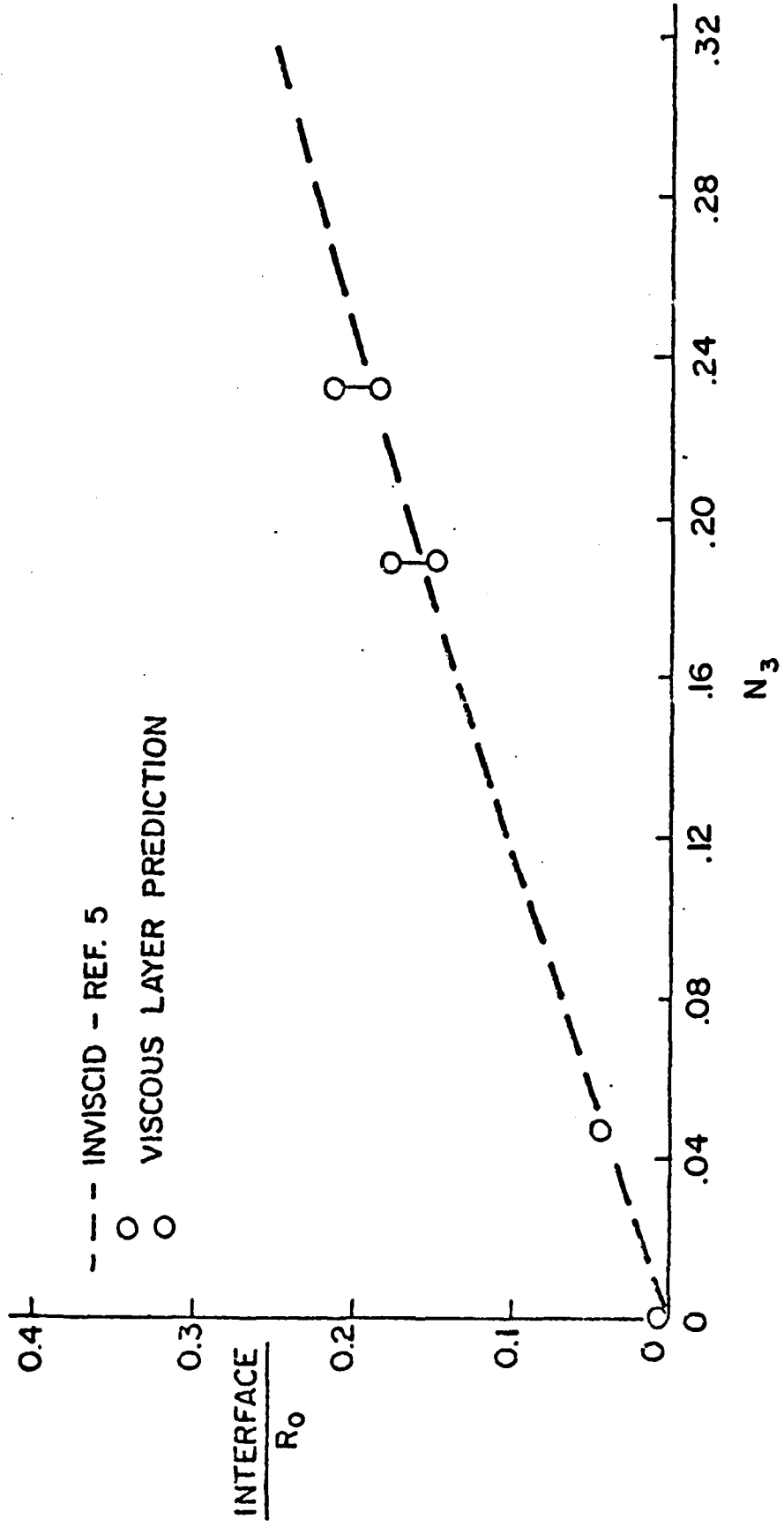


FIG. 7 INTERFACE VS N₃

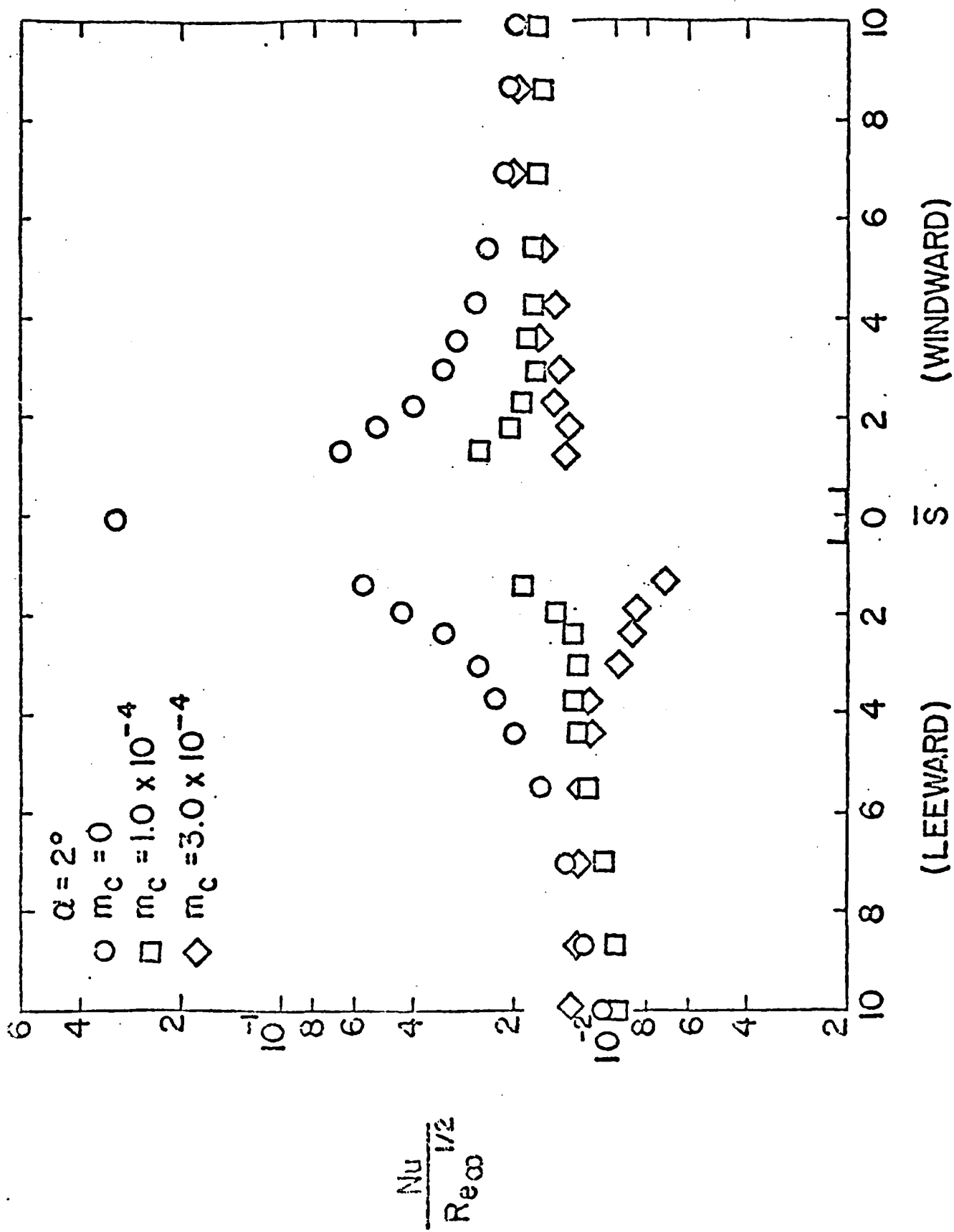


FIG. 8 NUSSELT NUMBER VS DOWNSTREAM DISTANCE ($\alpha = 2^\circ$)

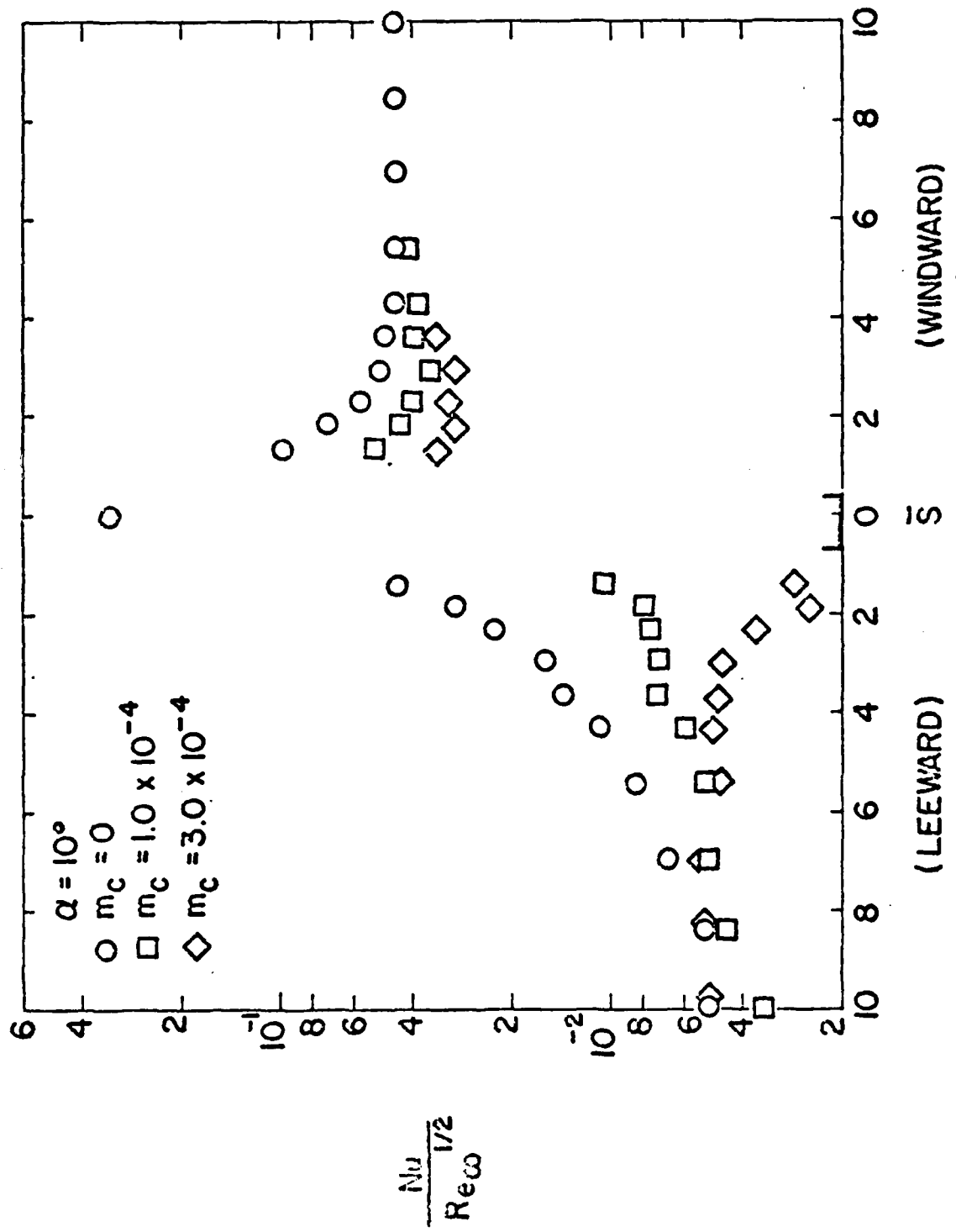


FIG. 9 HEAT TRANSFER DISTRIBUTION AT $\alpha = 10^\circ$

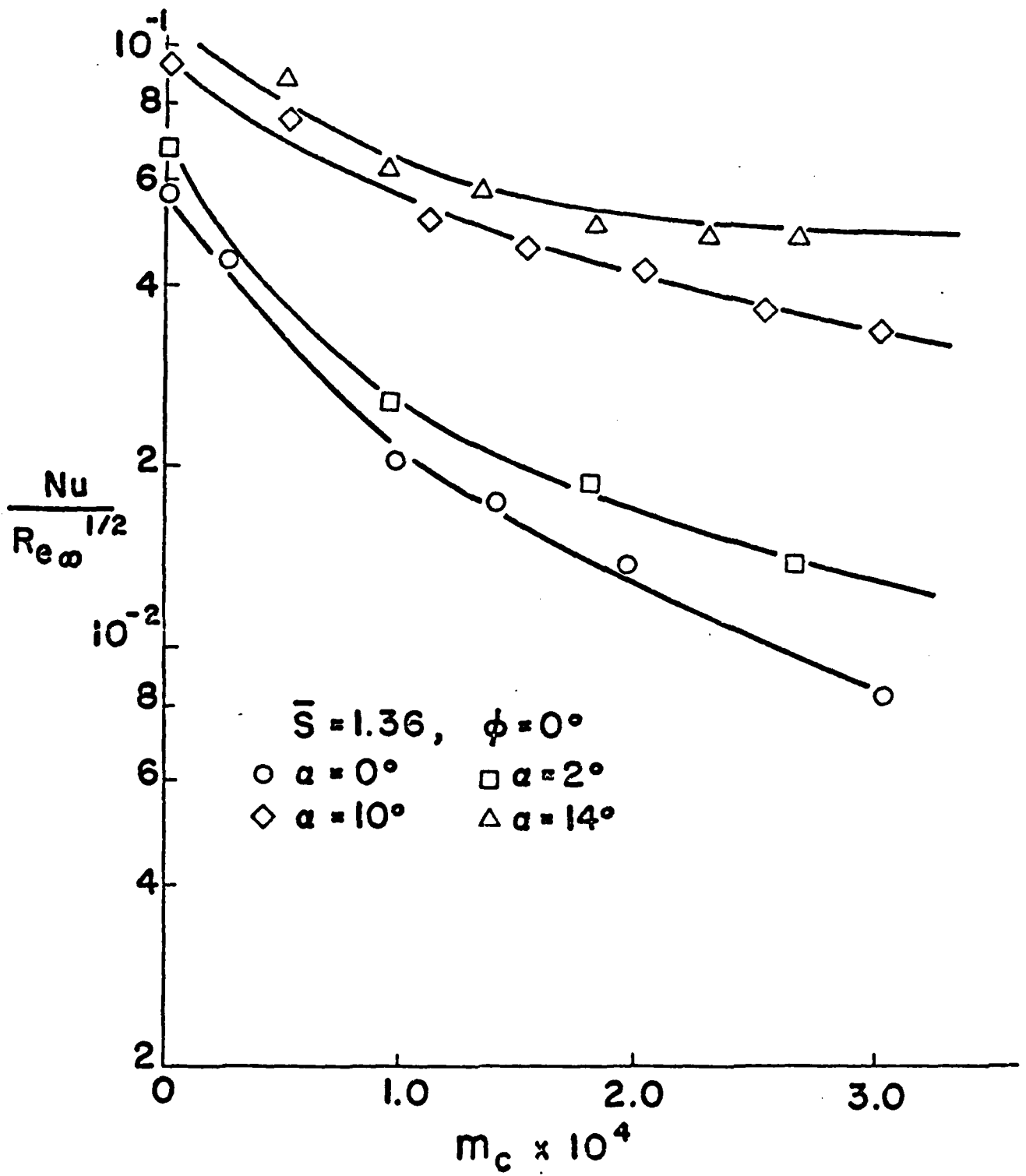


FIG. 10 NUSSELT NUMBER VS INJECTED MASS FLOW

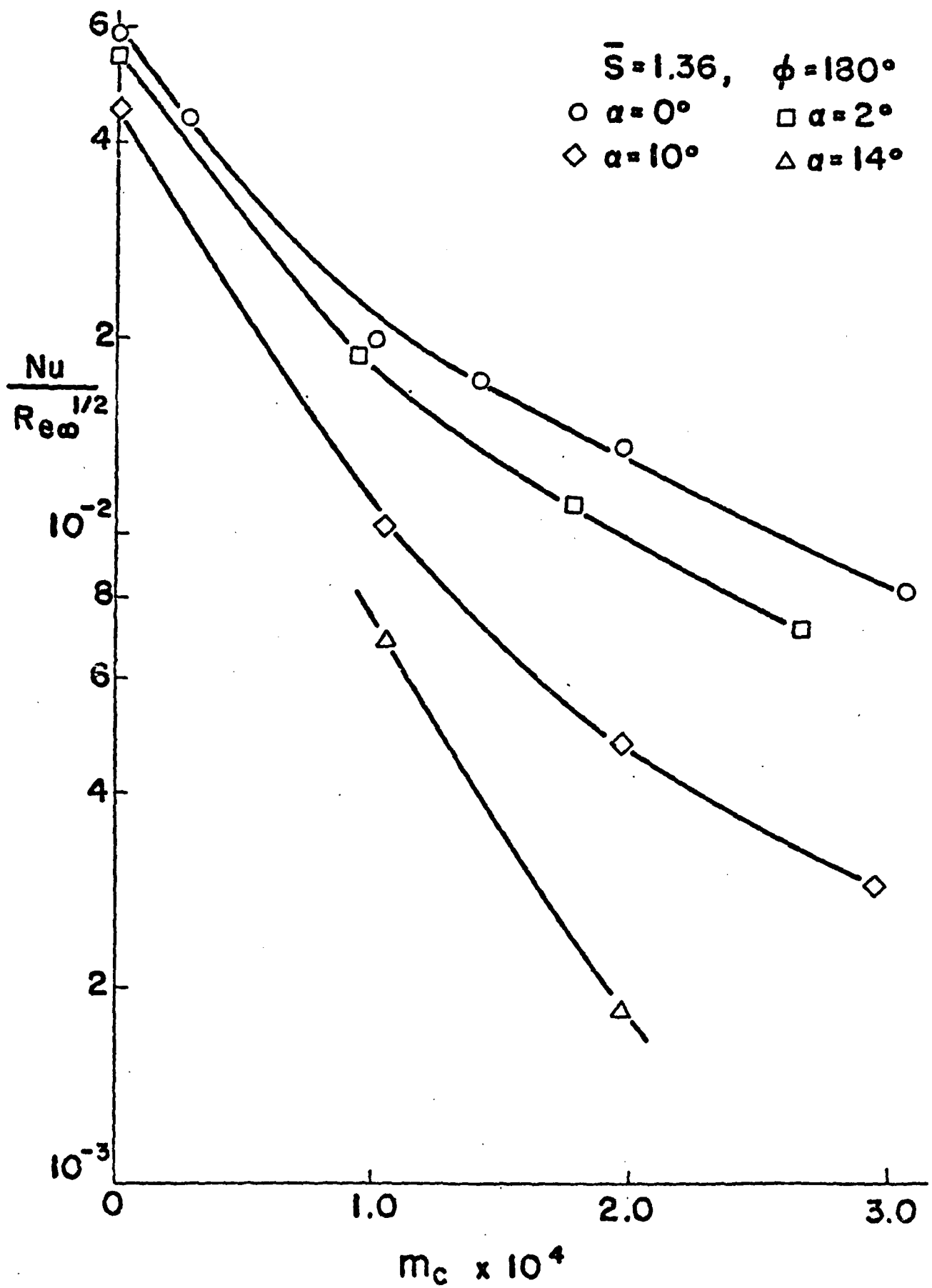


FIG. II NUSSELT NUMBER VS INJECTED MASS FLOW

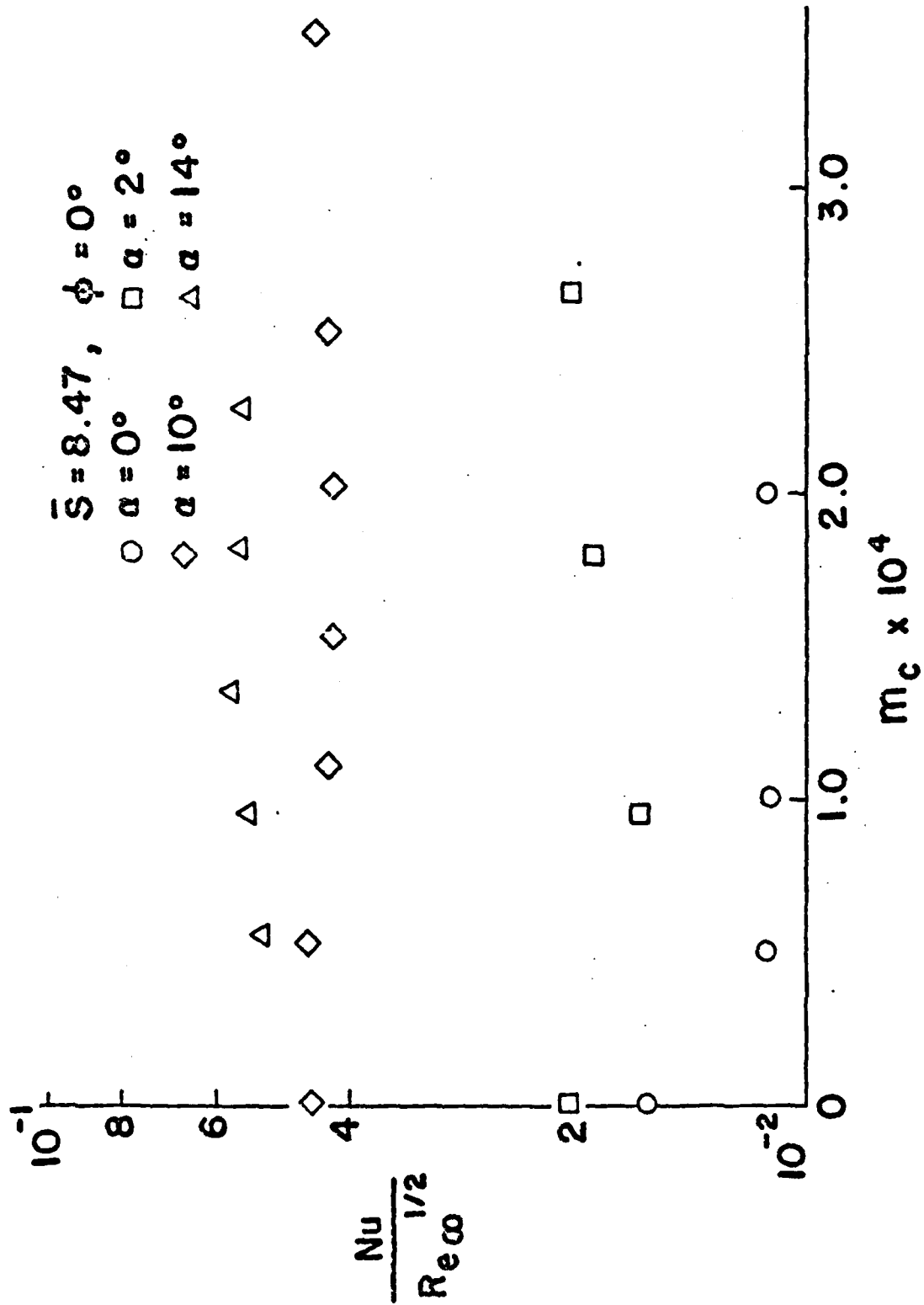
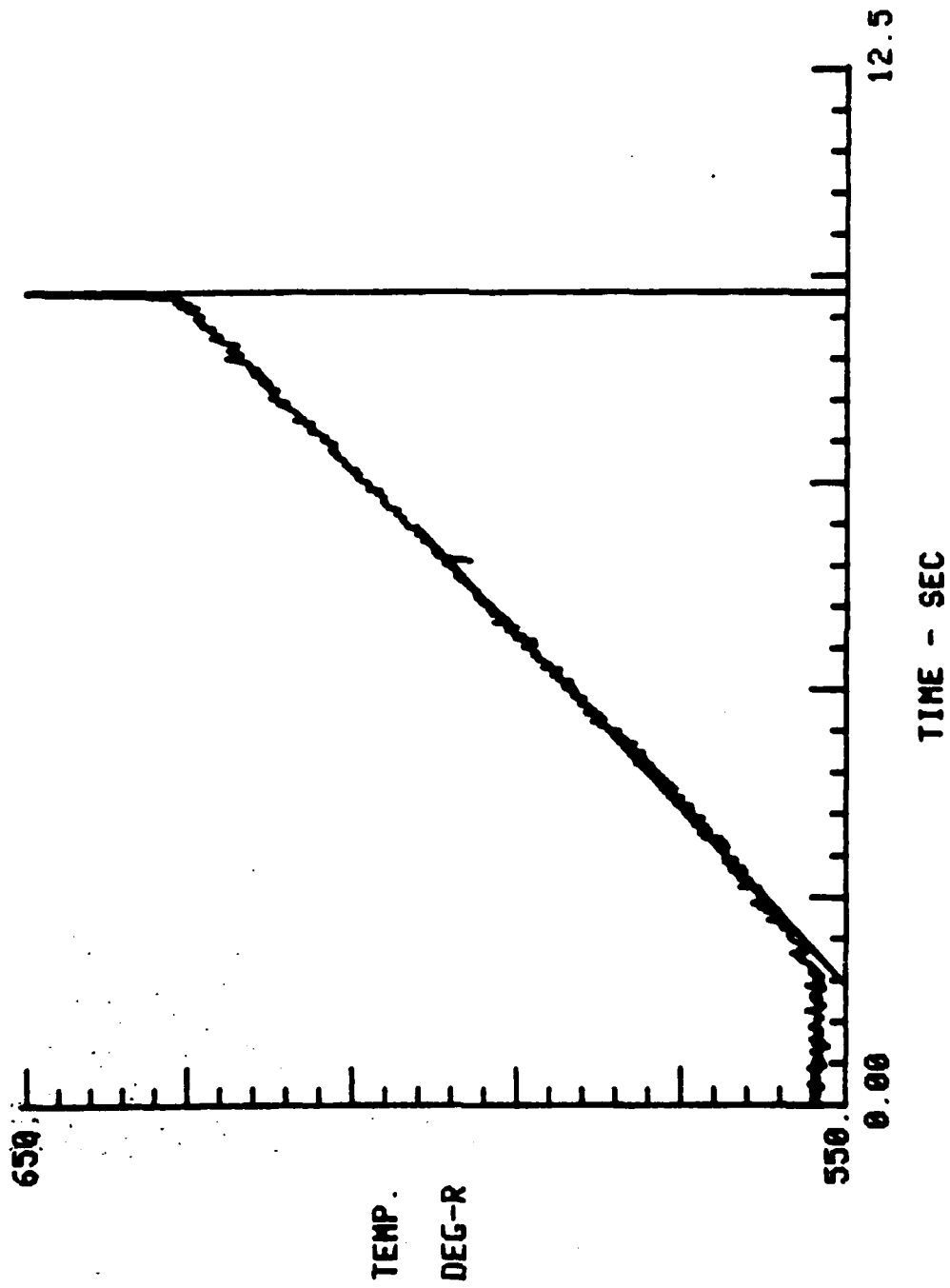
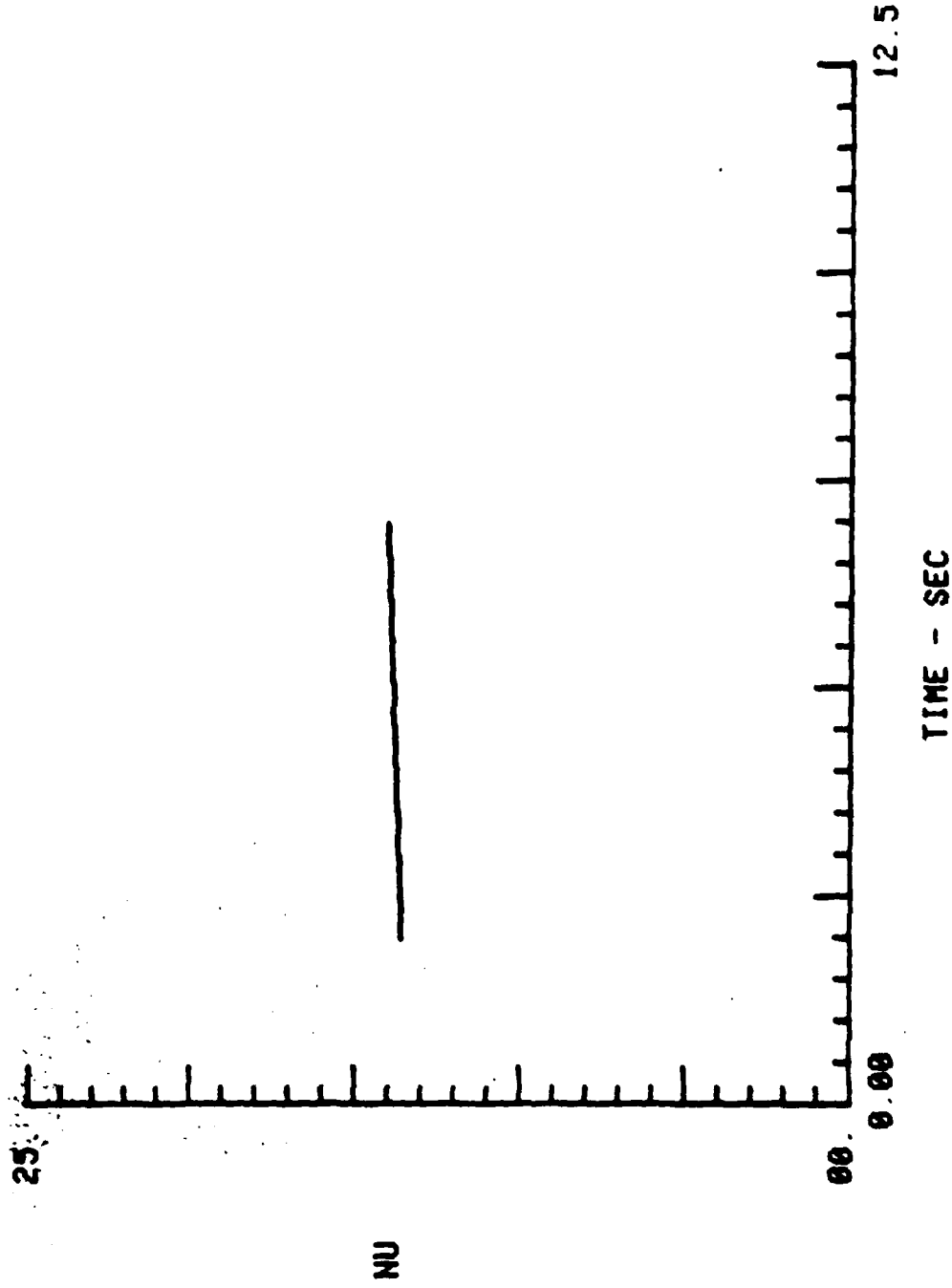


FIG. 12 NUSSELT NUMBER VS INJECTED MASS FLOW



TEST NO.= 30 DATE =09-10-80 TN= 2 S/RO=1.36

FIG. 13 MODEL SURFACE TEMPERATURE VS TIME



TEST NO. = 30 DATE = 09-10-80 TN= 2 S/RO=1.36

FIG. 14 NUSSELT NUMBER VS TIME

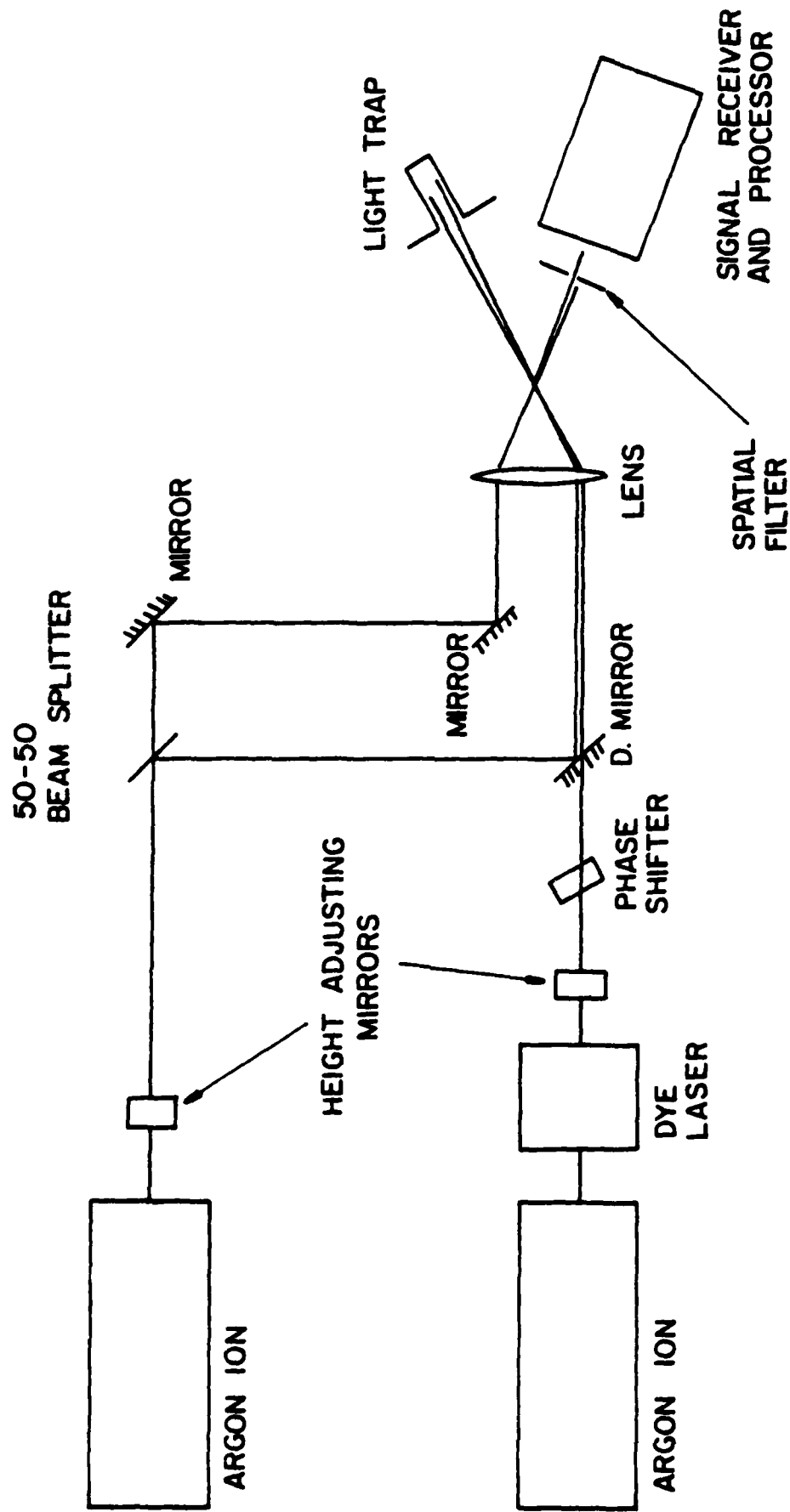


FIG. 15 SCHEMATIC DIAGRAM OF C-W CARS SYSTEM

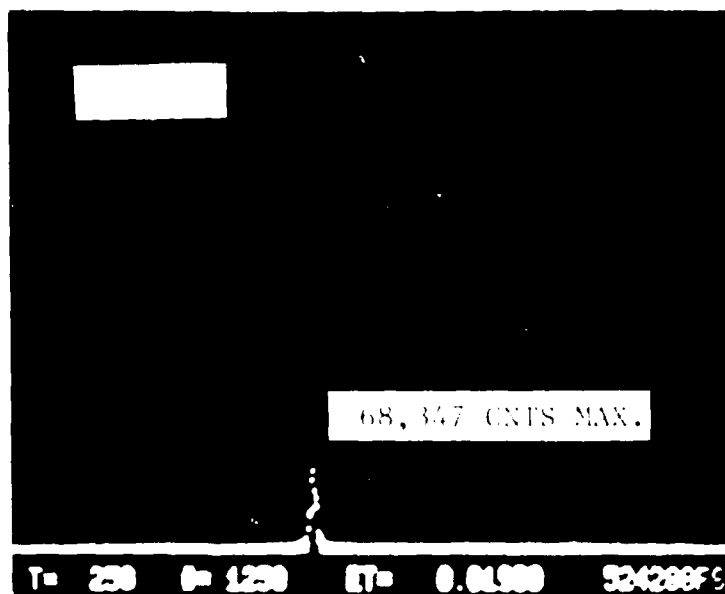


FIG. 16 ATMOSPHERIC WATER VAPOUR

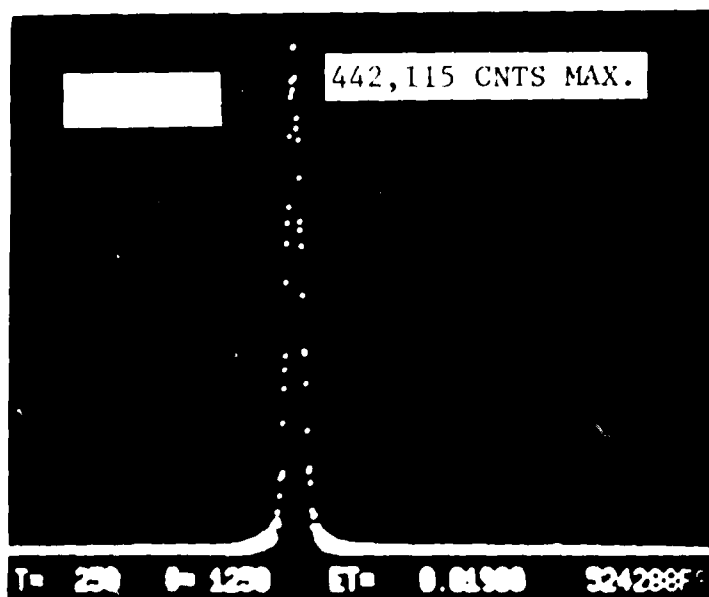
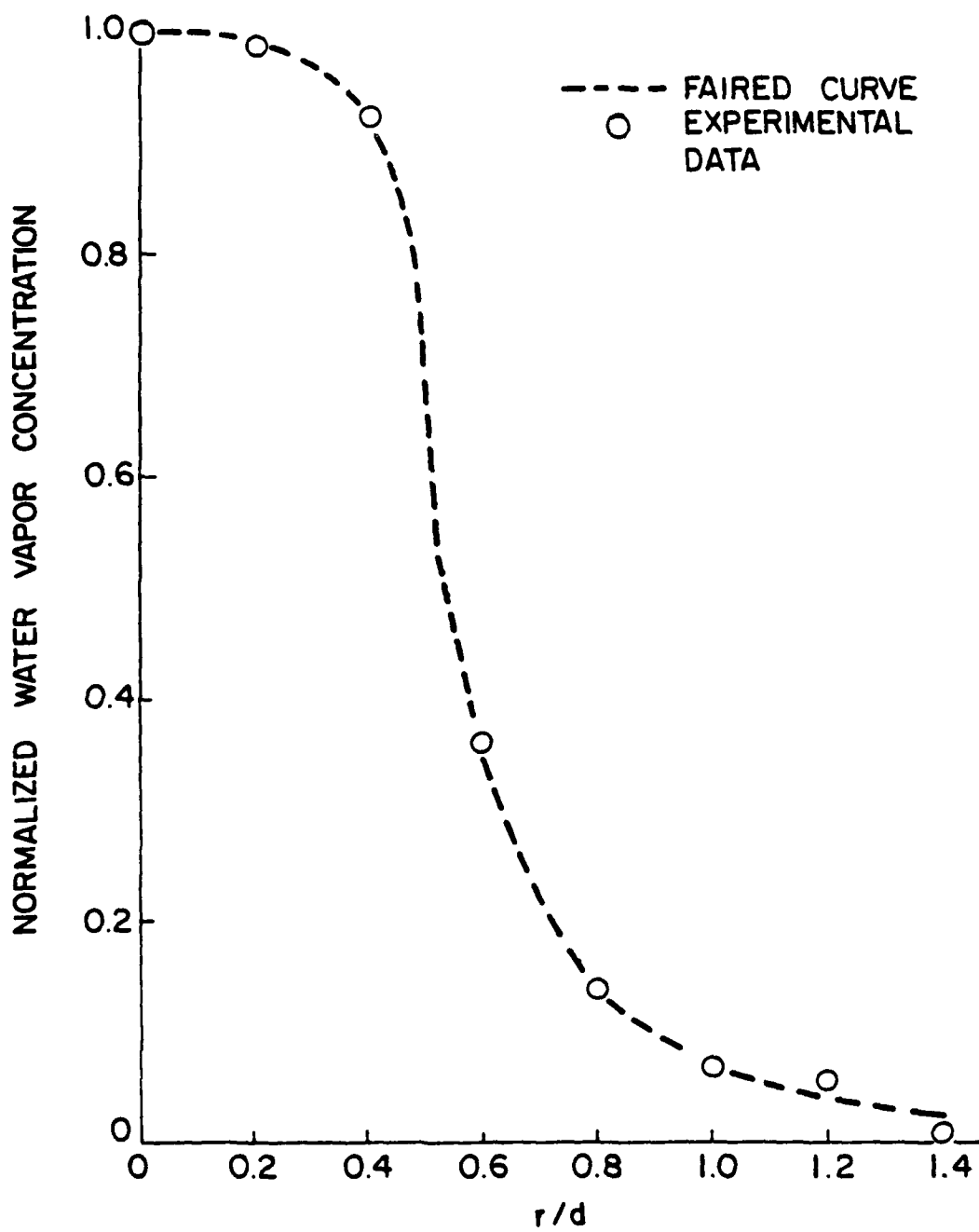


FIG. 17 WATER VAPOUR ABOVE BOILING WATER IN THE ATMOSPHERE



**FIG. 19 STEAM JET RADIAL PROFILE
AT $x/d = 1.0$**

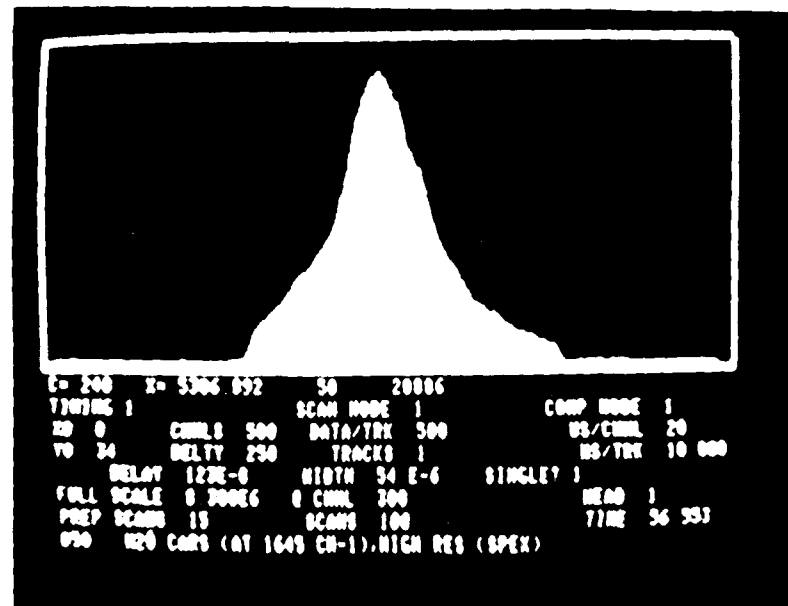
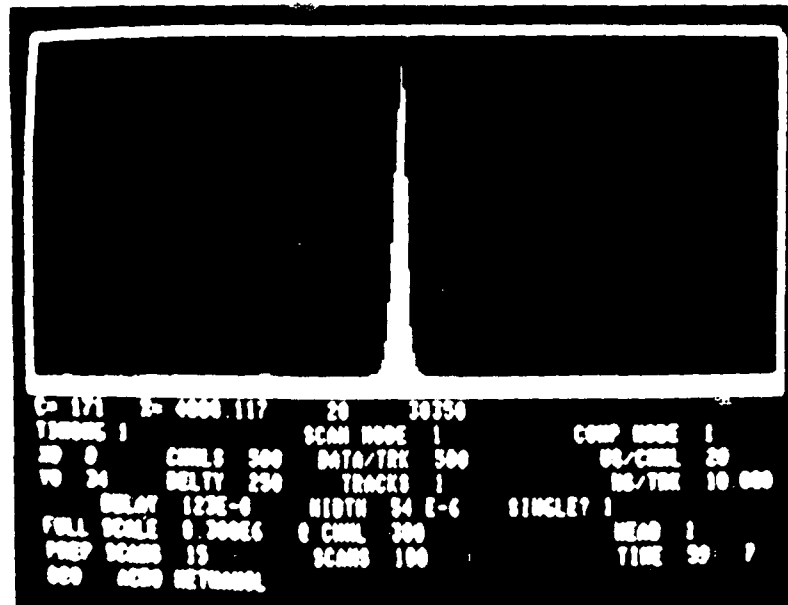


FIG. 20 CARS SIGNAL OF LIQUID WATER



**FIG. 21 PHOTOGRAPHIC VIEW OF CARS
ARRANGEMENT FOR LIQUID WATER
IN A CYLINDER**

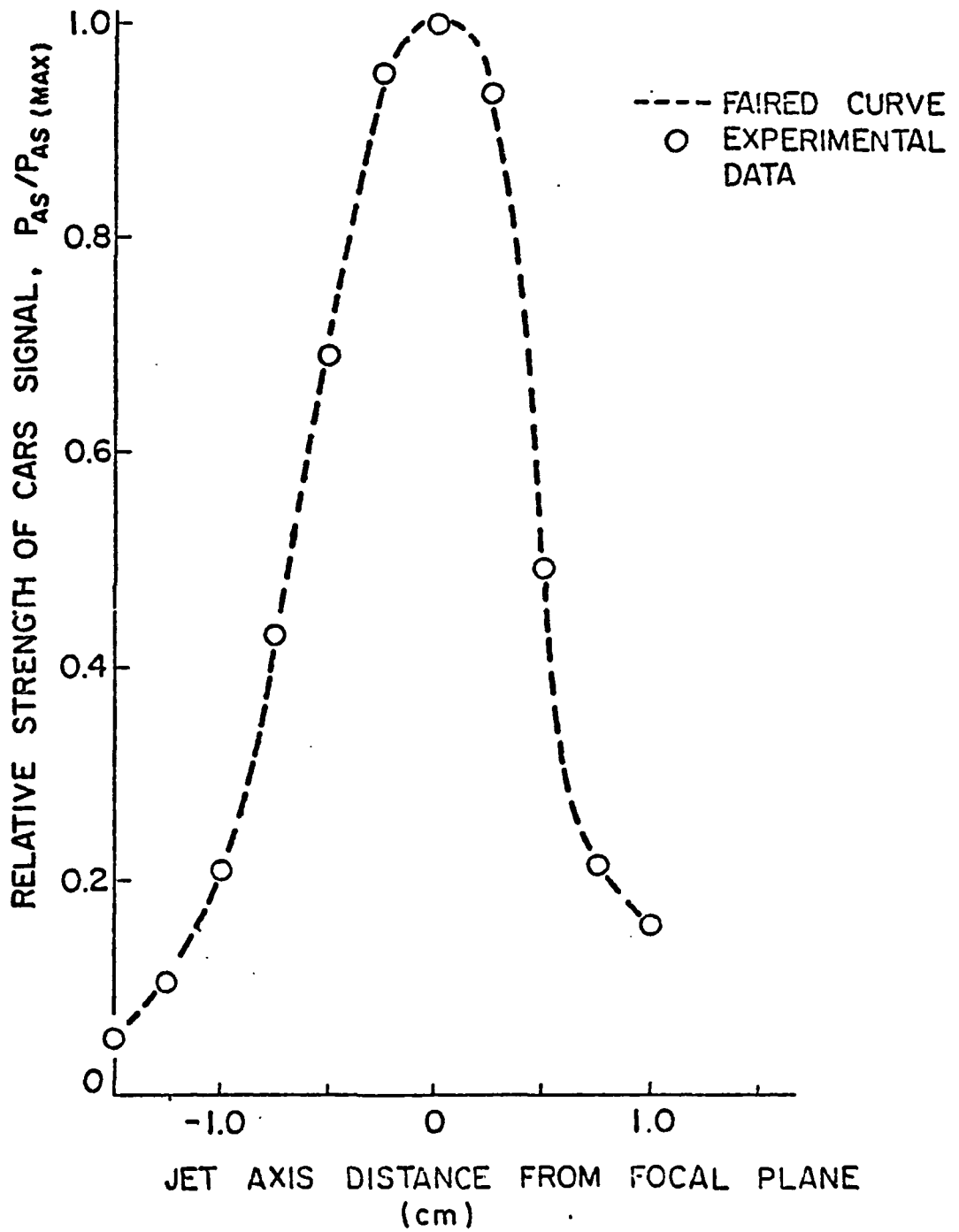


FIG. 22 CARS SIGNAL DECAY WITH FOCAL PLANE DISPLACEMENT

APPENDIX A

THREE-DIMENSIONAL VISCOUS INTERACTIONS

by S. G. Rubin

A combination of analysis and numerical methods has been considered in order to calculate flow properties on a variety of aerodynamic configurations; in addition, several model problems have been chosen in order to accurately and efficiently develop procedures to evaluate the viscous interacting flow over geometries having corners (junctures), edges (wing tips) and strong secondary flow interactions and possible separation.

The analytic tools that have been developed during these investigations and which provide the basis for the applications described here include:

- (1) 3D Boundary Region Analysis including possible viscous displacement interaction, with application to sharp and blunt nose configurations.
- (2) Parabolized Navier-Stokes analysis including consideration of departure effects, with application to cone flow.
- (3) Viscous Slender Body Theory for free pressure interaction analysis and for secondary flow evaluation on fuselage and low aspect ratio wing-body configurations.

Complementing the analysis is a comprehensive investigation of innovative numerical methods that lead to improved computational accuracy, efficiency and convergence rates. This is particularly important for three-dimensional viscous flows, where computer times and storage can become quite large. In this regard the following procedures have been developed for the applications previously detailed.

(1) Higher-Order Spline Interpolation for boundary region studies, turbulent BL, mass injection, parabolized NS equations, including a highly efficient deferred-corrector iteration technique.

(2) A Coupled Strongly Implicit method for boundary region, parabolized Navier-Stokes, transonic flows, including a conjugate gradient accelerator.

During the period covered here the applicability of the theoretical models has been examined for several complex flow configurations. The numerical techniques have been developed and tested on prototype model problems. The results have been quite encouraging. A brief description of several different areas of research as excerpted from selected papers follows. A complete list of the references for the period covered herein and where further details are available is attached.

1. Spline Deferred-Corrector Interpolation

The present investigators have formulated various higher-order collocation techniques based on polynomial spline interpolation^(7,8) or Hermitian discretization procedures. Three-point formulations leading to fourth-order and sixth-order methods were considered. In order to obtain equal accuracy the higher-order methods require fewer mesh points when compared with second-order accurate finite difference techniques. This can mean a reduction in computer storage and time. In particular, the fourth-order accurate spline 4 method⁽⁷⁾ generally requires one-quarter the number of points, in each coordinate direction, compared to finite-difference solutions of comparable accuracy.

In addition to improvements in accuracy, these methods have certain desirable properties. The discrete equations remain block-tridiag-

onal in character. In view of the Hermitian formulation, where the derivatives are treated as unknowns, the application of derivative boundary conditions is somewhat more straightforward, and with non-uniform grids the deterioration in accuracy is less severe than with conventional finite-difference methods. For a single differential equation, finite-differences lead to a scalar tridiagonal system, whereas the higher order techniques are block tridiagonal; specifically, 2x2 blocks are required for the fourth order spline methods and 3x3 blocks for the sixth order Hermite systems. Consequently, for a given mesh the storage requirements become larger. The solution procedure therefore requires more operations and is more time consuming than the scalar algorithm usually applied for the tridiagonal finite-difference equations. However, for equal accuracy the spline methods require fewer points are therefore still more efficient.

In a more recent study⁽⁹⁾ some of the complexities associated with computer storage and the general spline solution procedure are eliminated. This is accomplished by "uncoupling" the higher-order correction from the coupled lower-order ("finite-difference") system of equations. The present method results in a significant reduction in computer storage. This simplicity is achieved by treating the higher-order accurate terms as explicit correctors to a modified finite-difference equation. This correction is evaluated in such a manner that the resulting procedure is consistent and unconditionally stable.

It should be noted that by uncoupling the spline or Hermite corrector and thereby reducing the size of the matrix blocks, it is now possible to obtain higher-order solutions and still maintain a large

degree of coupling between the dependent variables in a system of equations. In effect, the equations are coupled solely through the implicit or finite-difference like terms. This is particularly important in both boundary layer and Navier-Stokes calculations, as the rate of convergence is increased considerably when the equations are coupled. The rate of convergence does not appear to be as sensitive to the uncoupling of the higher-order spline terms.

The present method has been tested with several problems:

(1) the one-dimensional Burgers equations, (2) the potential flow over a circular cylinder, (3) laminar and turbulent boundary layers on flat plates,^(7,8) (4) the Navier-Stokes equations describing the incompressible flow in a driven cavity,⁽⁹⁾ (5) the flow in a channel having a rearward facing step^(10,11) and (6) the viscous flow over a circular cylinder.^(10,11) For these latter investigations the coupled $(\Psi-\omega)$ Navier-Stokes equations are considered and Stone's strongly implicit method is extended to allow for the iterative spline correction. In all of the problems considered, the solution procedure is considerably simplified over that required for the coupled spline solvers; the final results are of course identical with both the iterative spline and coupled spline methods. The details of the corrector method, stability considerations, and typical calculations are given in reference 9.

2. Coupled Calculation Procedure

A numerical solution procedure for the Navier-Stokes equations in vorticity-stream function form has been considered. In the past, almost all explicit and implicit numerical systems that have been developed for these equations have been solved iteratively. It has generally been observed that for stability purposes, a nearly con-

verged solution of the Poisson equation for the stream function is required at each time level before incrementing the vorticity equation one time step. In order to accelerate the rate of convergence to the steady-state, SOR procedures, modified ADI techniques, strongly implicit methods and direct solvers have been considered for the solution of the Poisson equation. For the vorticity transport equation, explicit integration procedures are very time consuming and the temporal increment is restricted by the CFL condition. Implicit methods, though unconditionally stable, usually exhibit spurious oscillations and/or instability for large time steps and/or large cell Reynolds numbers. Moreover, the inversion of the governing tridiagonal system is only assured if the conditions for diagonal dominance (Courant number less than one and cell Reynolds number less than two) are satisfied. The addition of artificial viscosity or the use of upwind differencing (which also contains large amounts of artificial viscosity) usually assures diagonal dominance, but lowers the over-all accuracy or adds excessive numerical diffusion. Furthermore, in many instances, it has been necessary to underrelax in the initial stages of the calculation in order to obtain a converged solution. This is a very time-consuming process.

In the present study, ^(10,11) Stone's strongly implicit method is reformulated to allow for the solution of a 2x2 coupled system of equations. The vorticity-stream function form of the Navier-Stokes equations, with second-order accurate centered differences, is solved by this coupled strongly implicit procedure. The solution algorithm also allows for the coupling of the boundary conditions on the stream

function and vorticity in both coordinate directions. Solutions for arbitrary large time steps ($\Delta t \approx 10^6$) and cell Reynolds numbers much greater than two are possible. Results have been obtained without adding artificial viscosity and without the necessity of underrelaxation. Even with rather arbitrary initial conditions, the method converges quite rapidly to the steady-state solution, when one exists. A further improvement may be possible with a new gradient algorithm. (12)

The strongly implicit procedure has been used to solve for a variety of flow problems at moderately large laminar Reynolds numbers, generally $R_e \leq 2000$. The flow in a driven cavity, the associated temperature field in the cavity, the flow in a channel with a rearward facing step, the flow over a finite length flat plate, and the flow over a circular cylinder have been considered. Typical results for the step and cavity geometries are shown in figures A1-A4. The solution procedure is currently being evaluated for flow over cones at incidence.

3. Parabolized Navier-Stokes Equations

Hypersonic low density flows are characterized by the formation of a so-called merged layer in the region of the leading edge, where the inner viscous or boundary layer and the outer shock structure are virtually indistinguishable. Standard asymptotic methods are not easily applied and therefore Rudman and Rubin (1968) postulated the existence of a composite single layer system of equations that is uniformly valid throughout the merged region. This composite system of reduced equations represents the parabolic version of the Navier-Stokes equation. (13) A true initial value problem results and numerical marching procedures apply. Solutions were ob-

tained for flat plate, corner, conical and wing-tip geometries, by Lin and Rubin (1973).

For supersonic flows or for any configuration where upstream influences are important the p_x term in the axial momentum equation changes the purely parabolic character of the equations and introduces an "elliptic-like" effect that is reflected in the appearance of the so-called branching or departure solutions associated with forward marching procedures. The subsonic pressure interaction introduces an upstream zone of dependence; however, unlike fully elliptic problems, this zone appears to be of finite extent. Lin and Rubin⁽¹⁴⁾ have discussed various numerical approximations for the p_x term. These include specifying p_x , say from experimental data, using a retarded or backward difference, or applying a sublayer or boundary layer approximation, $p_y = 0$, in the subsonic wall region. All but the first approximation eventually encounter some type of instability. More recently, Lin and Rubin⁽¹⁴⁾ have considered a local (stepwise) time-dependent iteration in order to hyperbolize the system and thereby filter the departure effect. For example, in the two-dimensional flow case, the momentum equation becomes

$$u_t + uu_x + vu_y = -p_x/\rho + (\mu u_y)_y/\rho$$

This formulation differs from a conventional time-dependent scheme in that a streamwise forward-marching procedure (i.e., step-by-step calculation) is still used. A temporal iteration or relaxation is introduced. The initial conditions are specified at $x = x_0$, $y \geq 0$ and $t \geq 0$ with the following conditions:

$$u(x_0, y, t) = u_0(x_0, y, 0)$$

After an estimation of the flow properties is made at $t = 0$ and $x = x_0 + \Delta x$ (e.g., by Taylor series extrapolation), the numerical computations are carried out to obtain the flow properties at $x = x_0 + \Delta x$ and $t = \Delta t$. The calculations continue until a steady-state solution is reached at $x = x_0 + \Delta x$; i.e., until

$$\frac{\partial}{\partial t} u(x_0 + \Delta x, y, t) = 0.$$

When convergence is obtained to some prescribed tolerance, the calculations proceed downstream to $x = x_0 + 2\Delta x$, etc. This procedure, even for small Δx , has been successful. Some typical solutions for a cone at incidence are shown in figures A5 and A6. A strongly implicit coupled procedure has been presented by Rubin and Khosla.⁽¹⁰⁾ Like the ADI method, this technique combines a "parabolized" marching step with an elliptic relaxation step and appears to be quite suitable for describing a variety of moderate Reynolds number flows with confined separation regions. This procedure is being developed for the compressible Navier-Stokes⁽¹¹⁾ and "parabolized" Navier-Stokes equations. A typical result is shown in figure A7 for a step-like or boattail configuration. With this fully coupled relaxation procedure a smooth "departure-free" solution is obtained. This procedure can also be applied for bodies at incidence.

4. Internal Flows

The three approximations to the full Navier-Stokes equations usually described for external flows, i.e., interacting boundary layer/region, parabolic Navier Stokes or "parabolized" Navier-Stokes, are also applicable to internal flow configurations. Due to the confined nature of such flows, the boundary layer growth is limited and it is necessary that global mass conservation be enforced at each

streamwise station. For many of the full Navier-Stokes solvers that are currently in use this is not always a trivial consideration. In fact, it would appear that to some extent the pressure-displacement interaction of external flows is replaced with a pressure-mass flux condition for internal flows.

Rubin and Khosla in an unpublished study have considered the two-dimensional extension of their viscous channel theory developed earlier for three-dimensional incompressible flows⁽¹³⁾ to compressible flows. Some rather interesting results have been obtained and these provide a second indication of the free interaction behavior resulting from the axial pressure - global mass conservation relationship. With the (ξ, x, y) scaling, the Reynolds number does not appear in the governing equations. A forward marching technique is applied with the axial pressure determined iteratively from mass conservation conditions. With subsonic initial conditions, e.g., a Mach number $M = 0.8$, the boundary layer grows as the flow accelerates subsonically; surprisingly, the marching procedure proceeds down the channel directly through sonic conditions without choking, and continues to accelerate supersonically until the now thinning boundary layer becomes less than one mesh point thick. The calculation could be continued with a finer mesh but this was not considered useful. The final nearly uniform channel Mach number was approximately $M = 1.4$. The centerline pressure, Mach number and velocity, and the Mach number profiles at various sections are shown in Figs. A8 and A9. These solutions in effect depict a transonic nozzle with a design test section having a Mach number of 1.4. The channel is straight and the flow is accelerated solely by viscous displacement effects. Of course, the channel would have to be extremely long for all but

the smallest Reynolds numbers. We recall that the normalized axial coordinate $\xi = 3(2x/R)^{1/2}$ or $x = \xi^2 R/2\beta^2$, therefore for $\xi = 1$, $\beta \approx 1$ $x \approx R/2$. Although the idea of designing such a "wind-tunnel" is intriguing, this is not the primary point of the present discussion. What has been demonstrated is the free interaction pressure-displacement behavior. The displacement boundary layer clearly adjusts to the pressure and vice-versa in order to allow a smooth sonic transition.

Finally, the "parabolized" Navier-Stokes system has been applied by Ghia et al. ⁽¹⁵⁾ to channels having small protuberances, but large enough to induce separation. A forward marching procedure is applied to the parabolic Navier-Stokes system, i.e. fixed pressure, and a second elliptic relaxation step is used to introduce the upstream influences ("parabolization"). Significantly, this "parabolized" Navier-Stokes model appears to provide results consistent with the recent theoretical analysis. It should be noted that extreme care in the development of the pressure boundary conditions is required in order to insure that pointwise and global mass conservation is satisfied. A more complete discussion and detailed solutions are given by Ghia et al. ⁽¹⁵⁾ The question of coordinate systems to be discussed in the following section is also addressed in this study. From these results, it should be possible to evaluate the importance of the normal pressure gradients and therefore to determine the applicability of the somewhat interacting boundary layer (region, in three-dimensions) approach to internal flows with limited separation regions or other upstream influences.

5. Wing-Body Secondary Flow Interaction

The applicability of slender-body theory for the evaluation of

three-dimensional boundary layer induced secondary flows has been established.⁽¹⁶⁾ Specifically, the incompressible viscous induced potential field over an elliptic cylinder has been determined. The validity of this procedure has been explicitly demonstrated with the results for the two limiting cases of the circular cylinder and the finite-span flat plate. The exact three-dimensional potential solution is known for the flat plate geometry and this result is reproduced by the quasi-two-dimensional slender body method.

It is shown that this viscous slender-body theory (VSBT) is applicable near the surface of the body, i.e., at the edge of the boundary layer, and when (1) the geometry is slender and smooth as required by the familiar inviscid theory, (2) the Reynolds number is sufficiently large so that the boundary layers are thin, and (3) separation regions are confined to small bubbles within the boundary layer. Geometries of particular interest satisfying these conditions include bodies of revolution at moderate incidence and three-dimensional low aspect ratio wing-body configurations. The theory fails locally when the axial or azimuthal curvature becomes very large, e.g., at the side edge of an ellipse as the eccentricity e approaches unity. This represents the tip of the plate or wing.

In the present study,⁽¹⁶⁾ the VSBT has been applied to a cylinder having a typical wing-body-tail cross-section. The objective is to demonstrate an efficient analytical procedure for the evaluation of induced secondary potential and boundary layer flows. The effects of very small angles of incidence are also considered. This technique can ultimately be combined with a more general

boundary layer calculation procedure in order to consider actual wing-body configurations of finite length and with longitudinal curvature. This becomes an alternative to full Navier-Stokes calculations at large Reynolds numbers.

This procedure is generalized by conformal mapping techniques to allow for more arbitrary cross-sections. Finally, a more efficient Green's function technique replaces the earlier Fourier series method for the potential flow solution. The number of resulting quadratures is greatly reduced.

Results are presented for different combinations of elliptical fuselage-horizontal wing-vertical tail cross-sections. Closed form potential flow solutions are possible for the circular fuselage-horizontal wing configuration. The other potential solutions are obtained by quadratures. Matched expansion techniques are applied for the evaluation of the secondary flow boundary layers. Small angles of incidence are also considered in the present study. Some typical results are shown in figures A10 and A11.

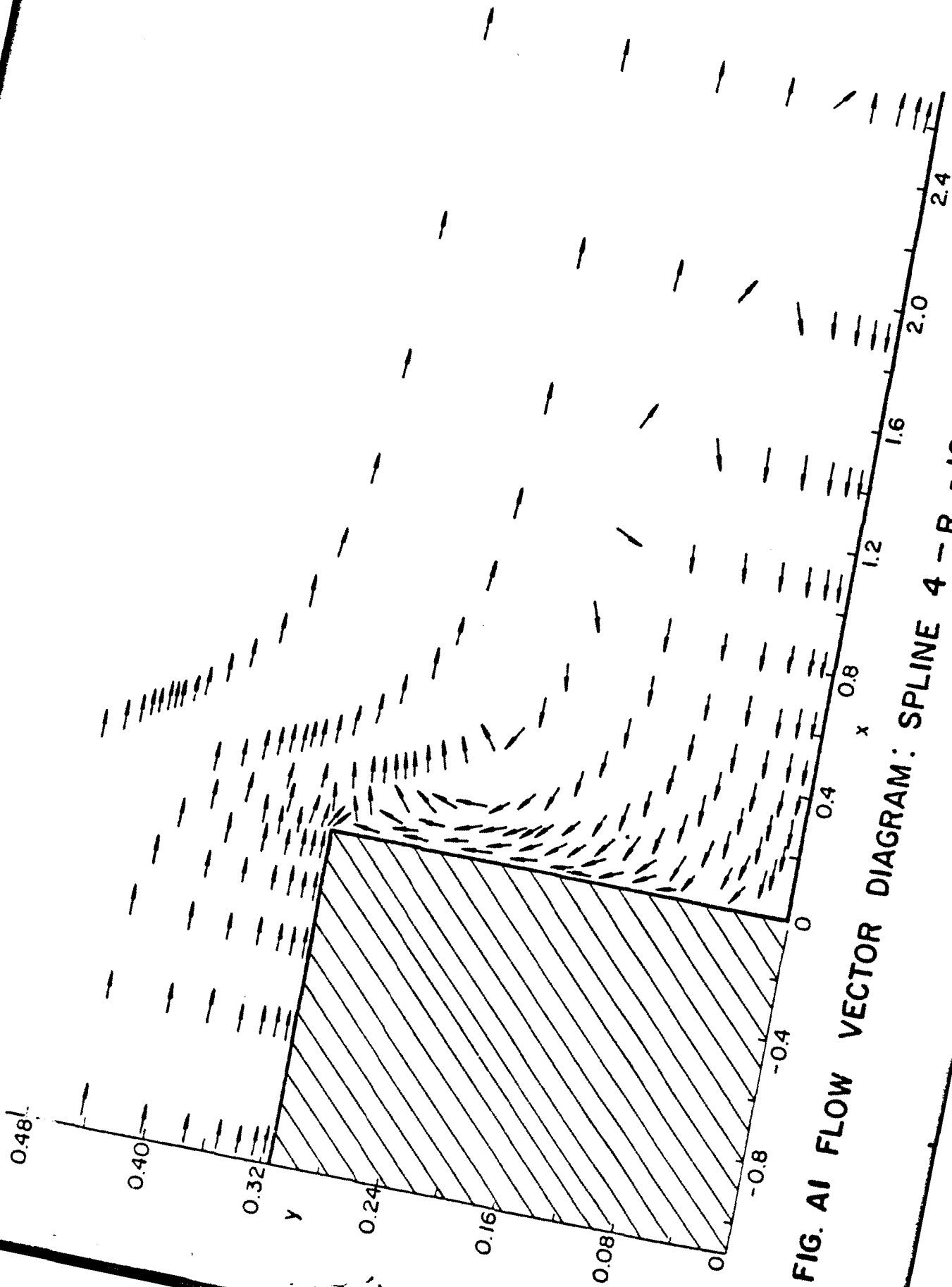


FIG. A1 FLOW VECTOR DIAGRAM: SPLINE 4 - $Re = 1000$

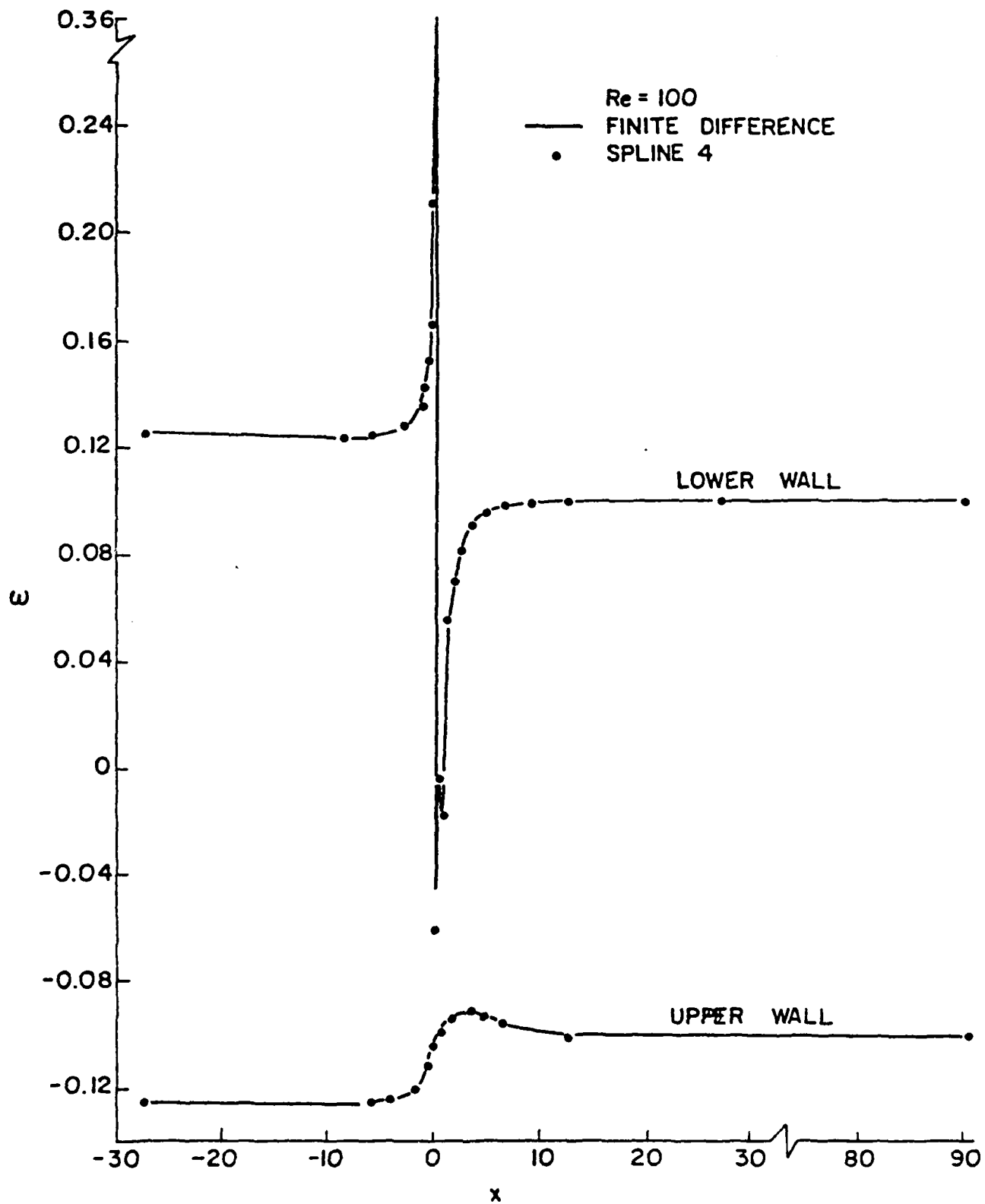


FIG. A2 WALL VORTICITY IN A CHANNEL

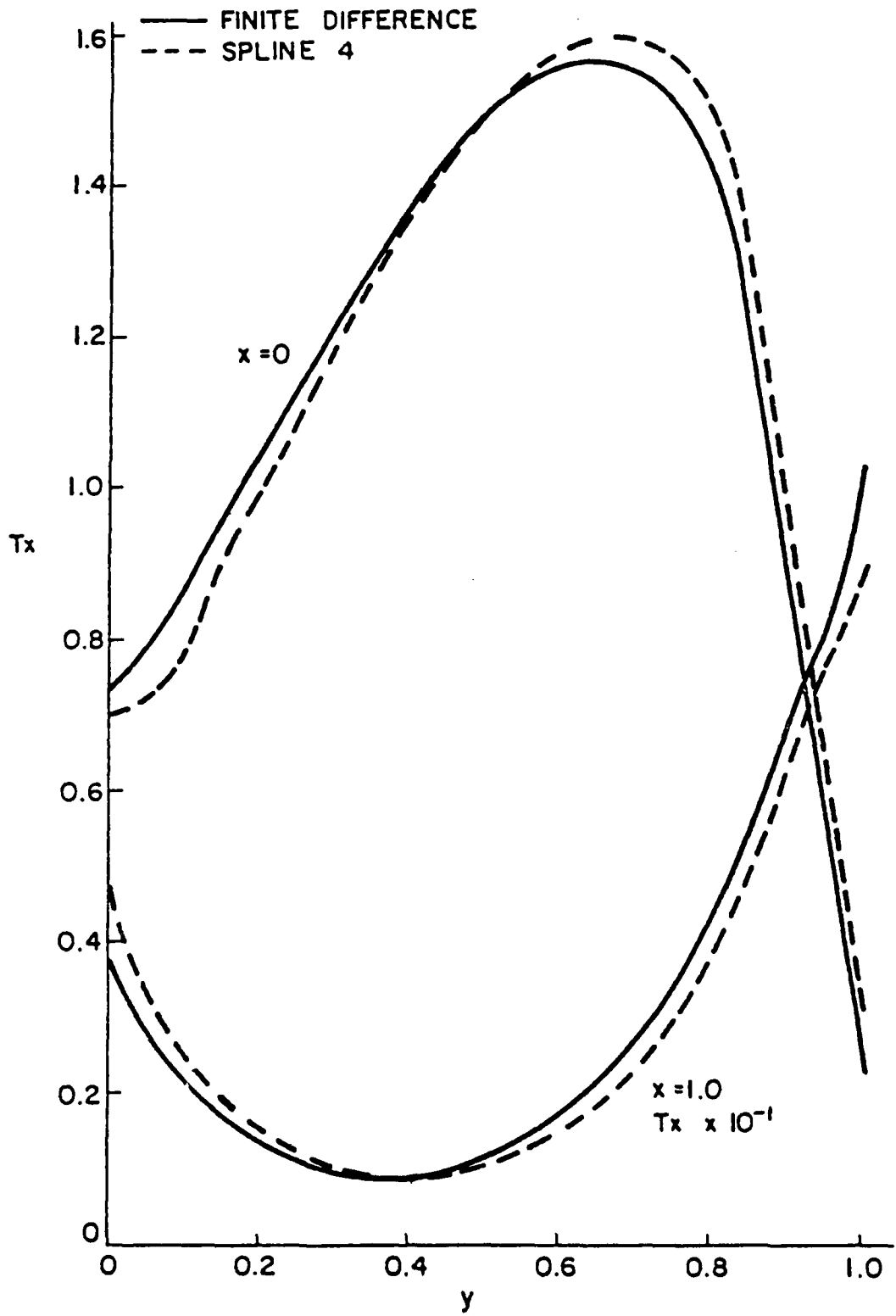


FIG. A3 HEAT TRANSFER ON SIDE WALLS OF CAVITY

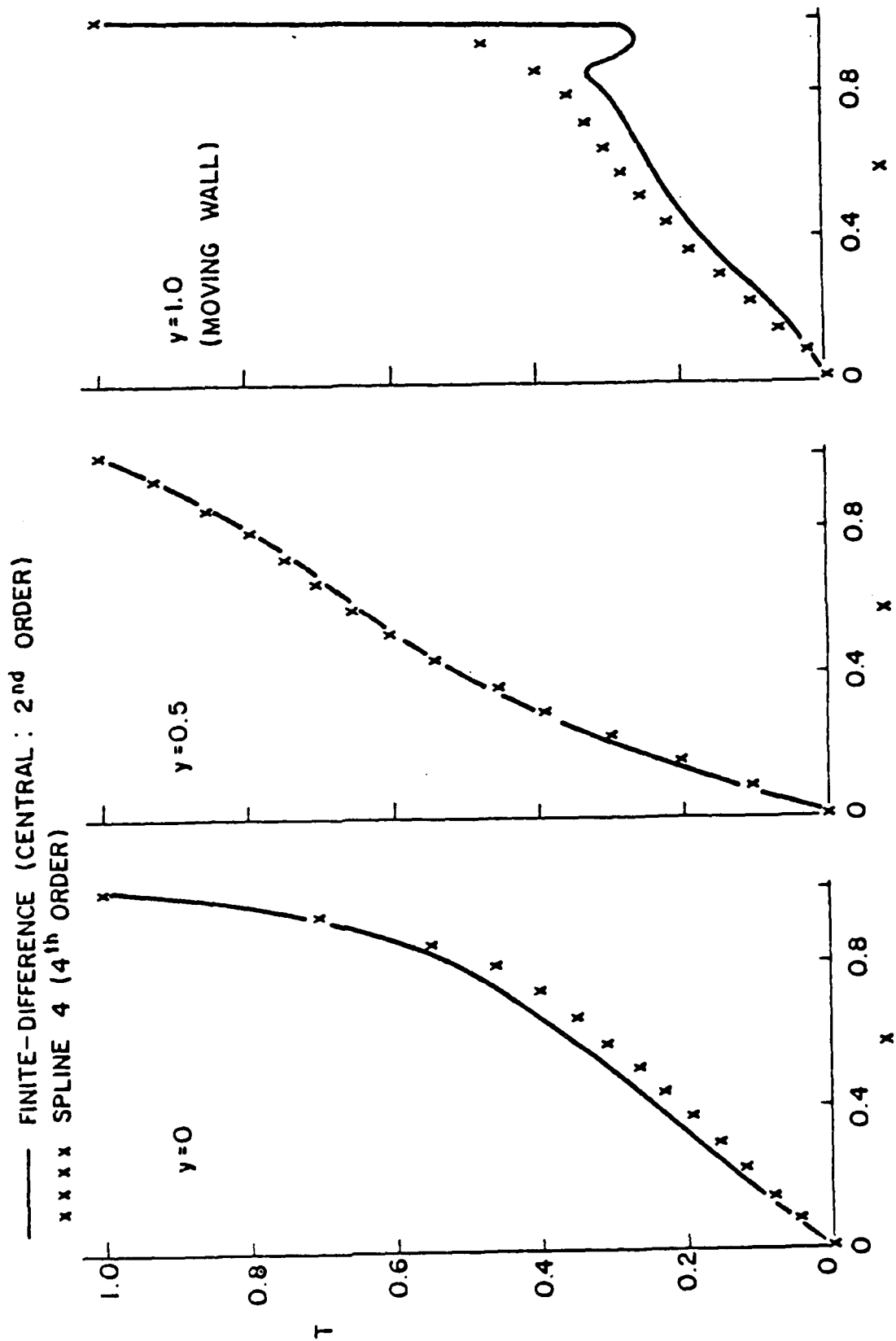


FIG. A4 TEMPERATURE PROFILES FOR DRIVEN CAVITY : PE = 50.

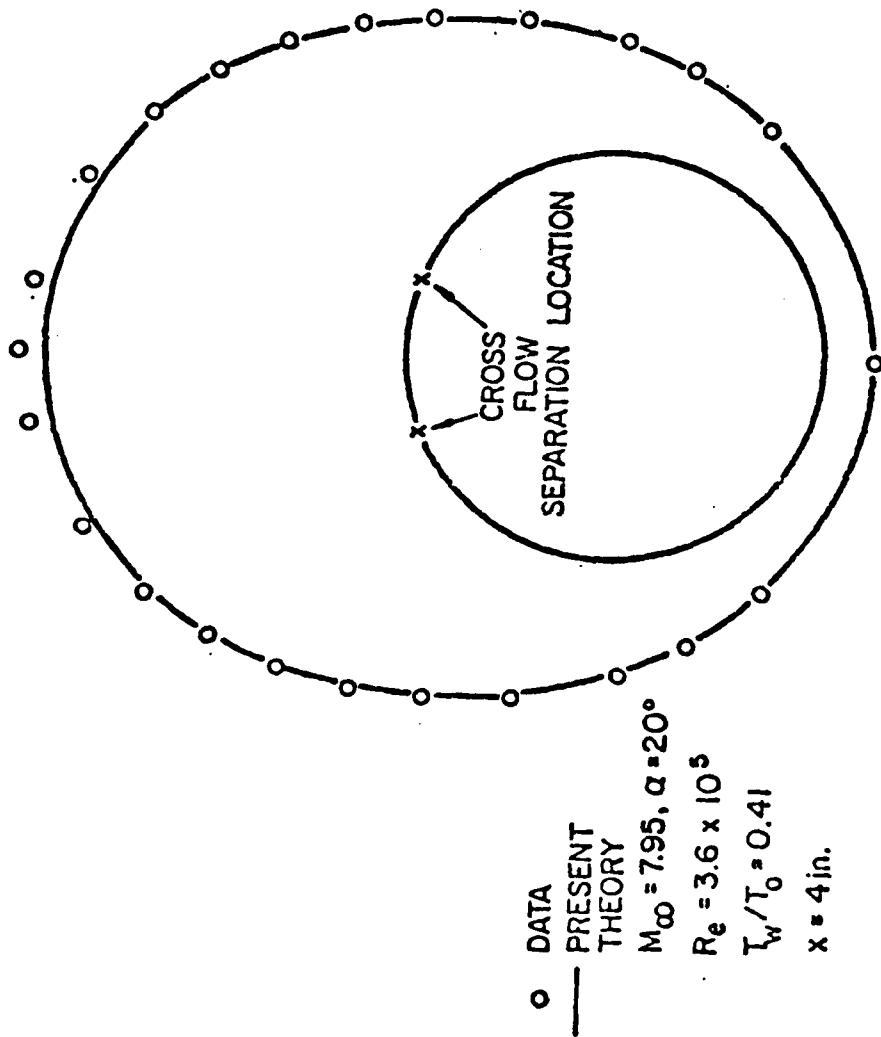


FIG. A5 CIRCUMFERENTIAL BOW SHOCK DISTRIBUTION FOR SHARP CONE (PNS), AFTER LIN AND RUBIN (1979)

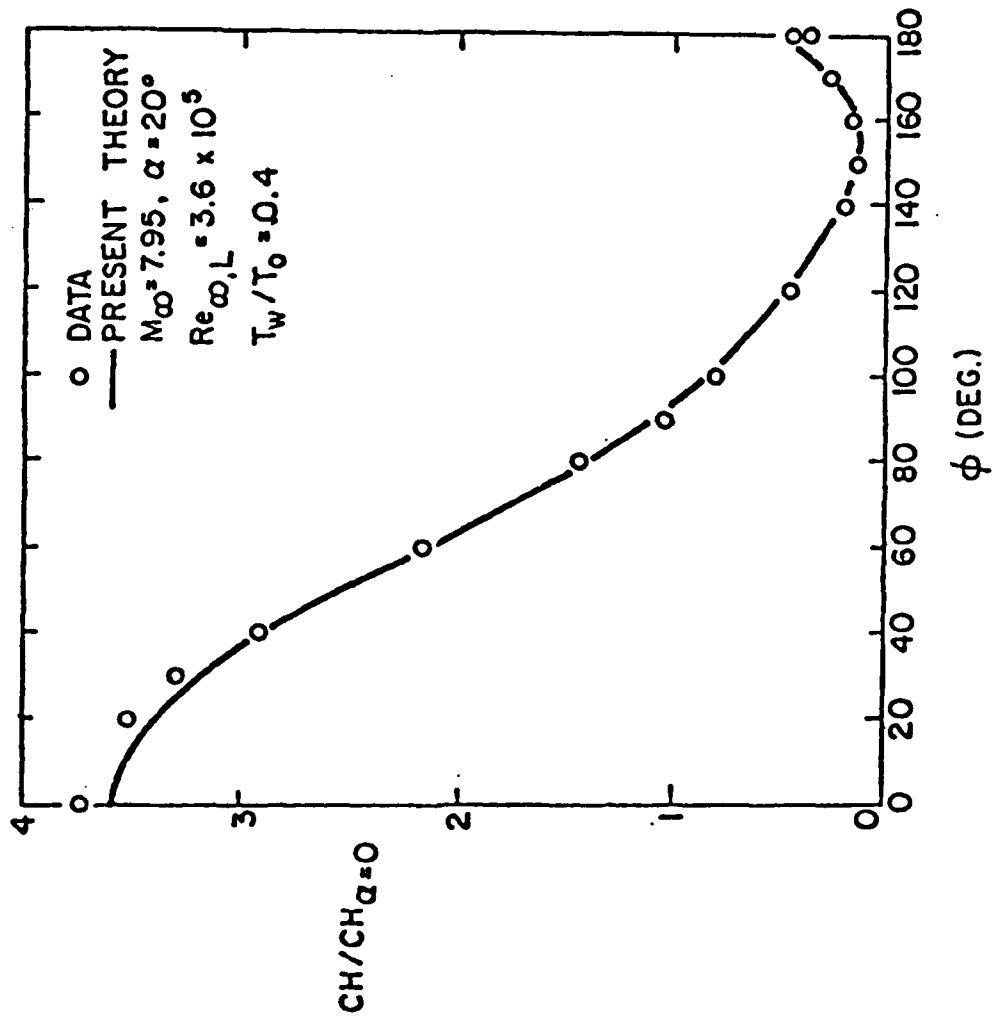


FIG. A6 CIRCUMFERENTIAL HEAT TRANSFER DISTRIBUTION
 ON SHARP CONE (PNS), AFTER LIN AND
 RUBIN (1979)

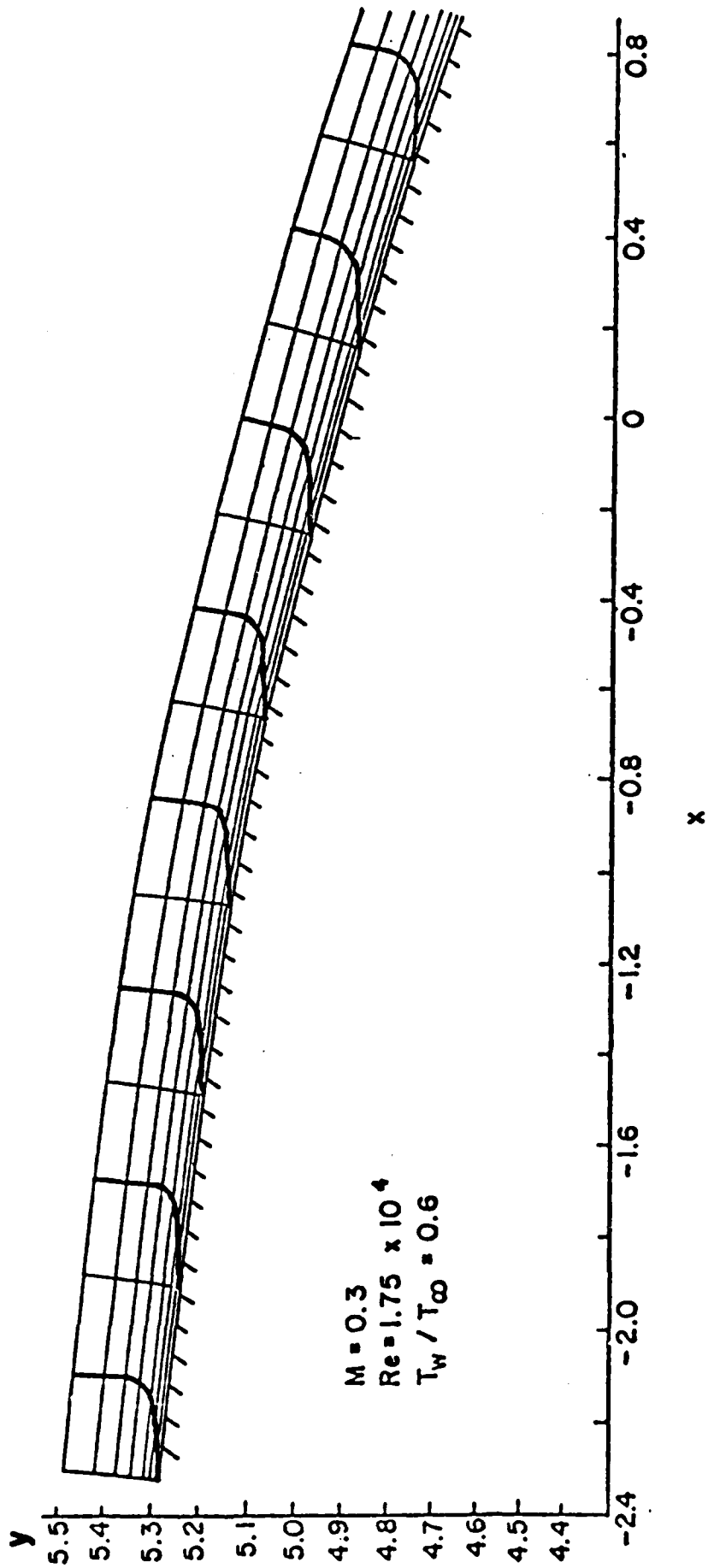


FIG. A7 COMPRESSIBLE NAVIER - STOKES SOLUTION FOR BOATTAIL SIMULATOR

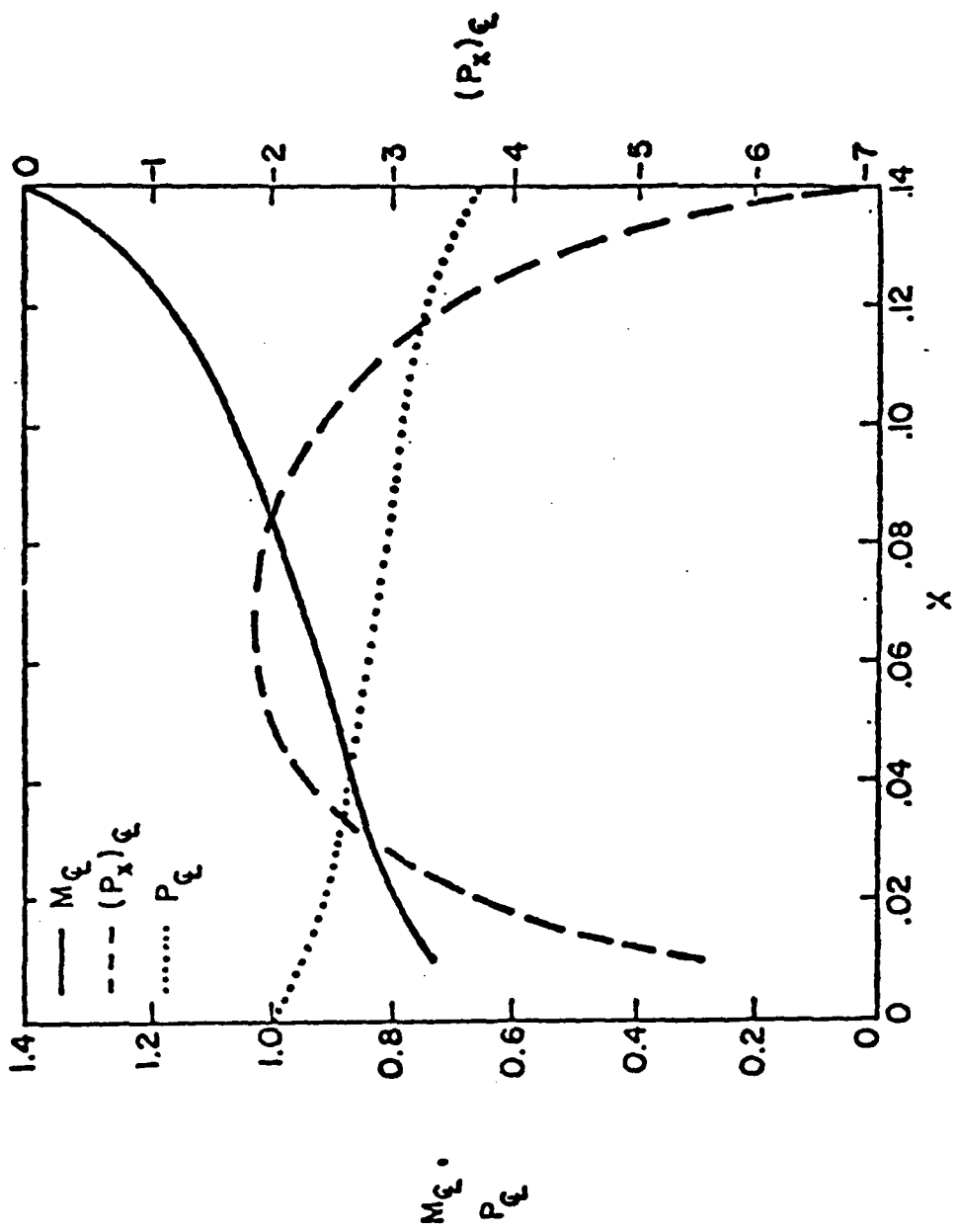


FIG. A8 CENTERLINE PROFILES - COMPRESSIBLE CHANNEL FLOW WITH PRESSURE INTERACTION

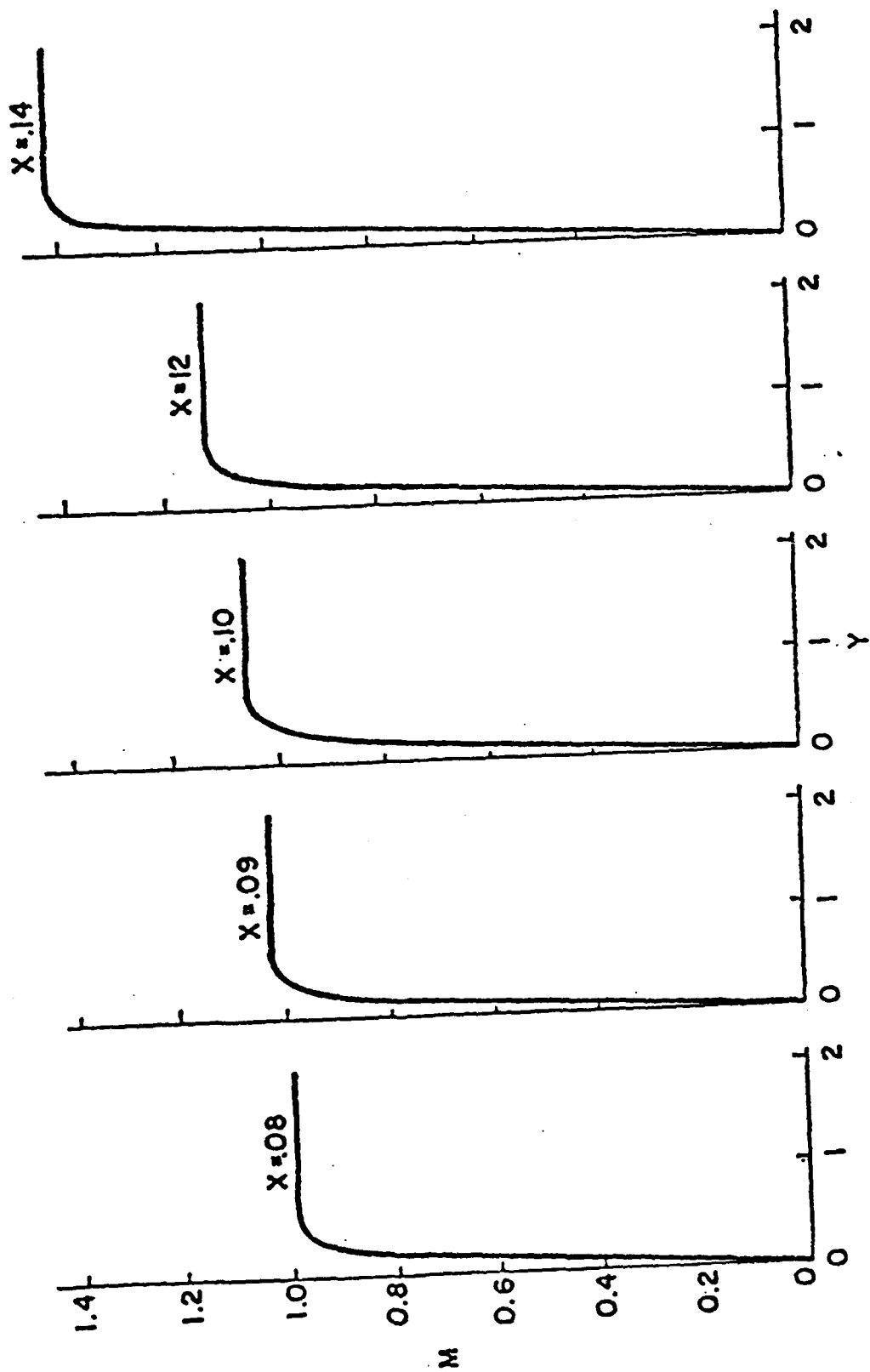


FIG. A9 MACH NUMBER PROFILES - COMPRESSIBLE CHANNEL WITH PRESSURE INTERACTION

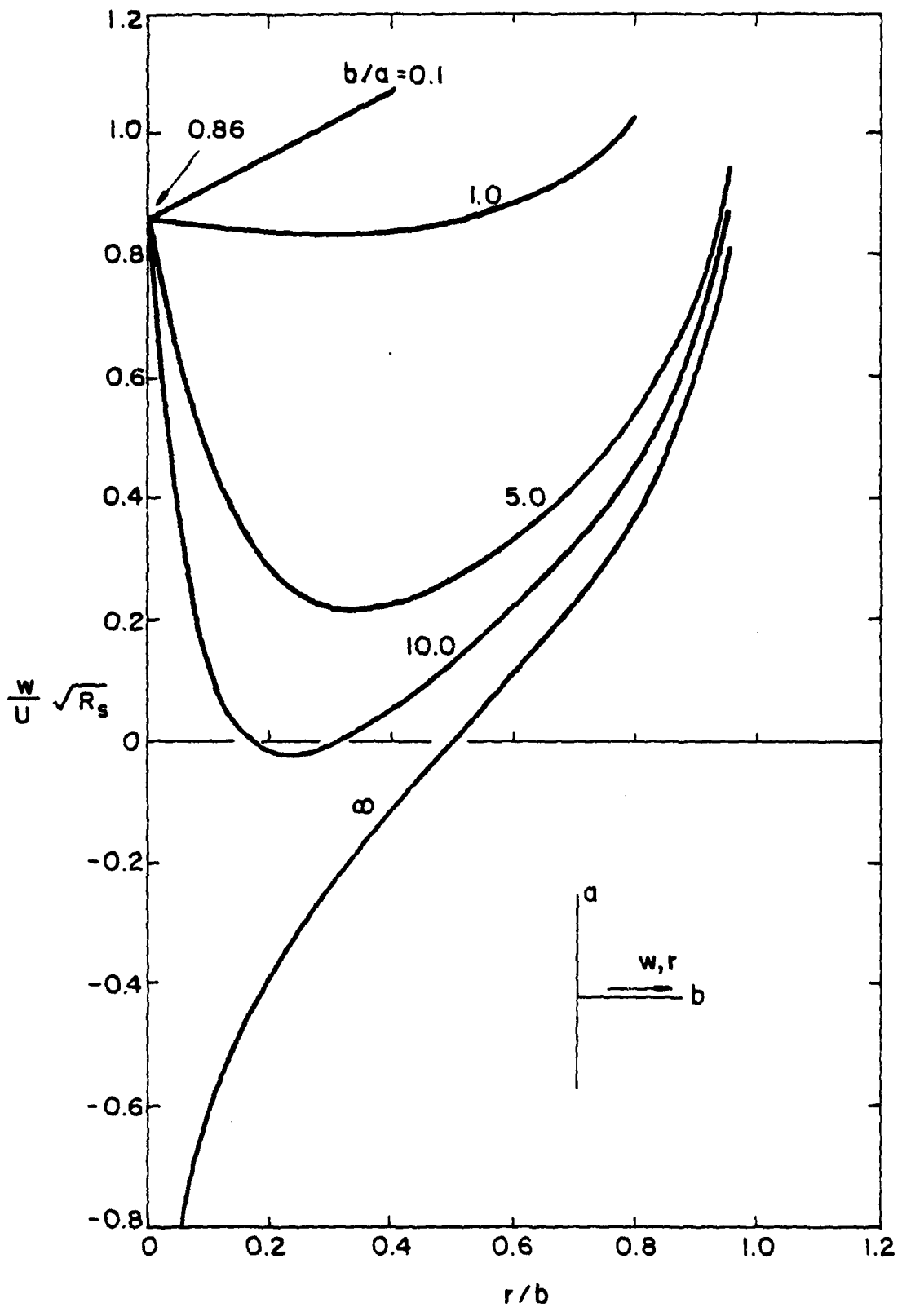


FIG. A10 WING-TAIL INDUCED CROSSFLOW: TAIL

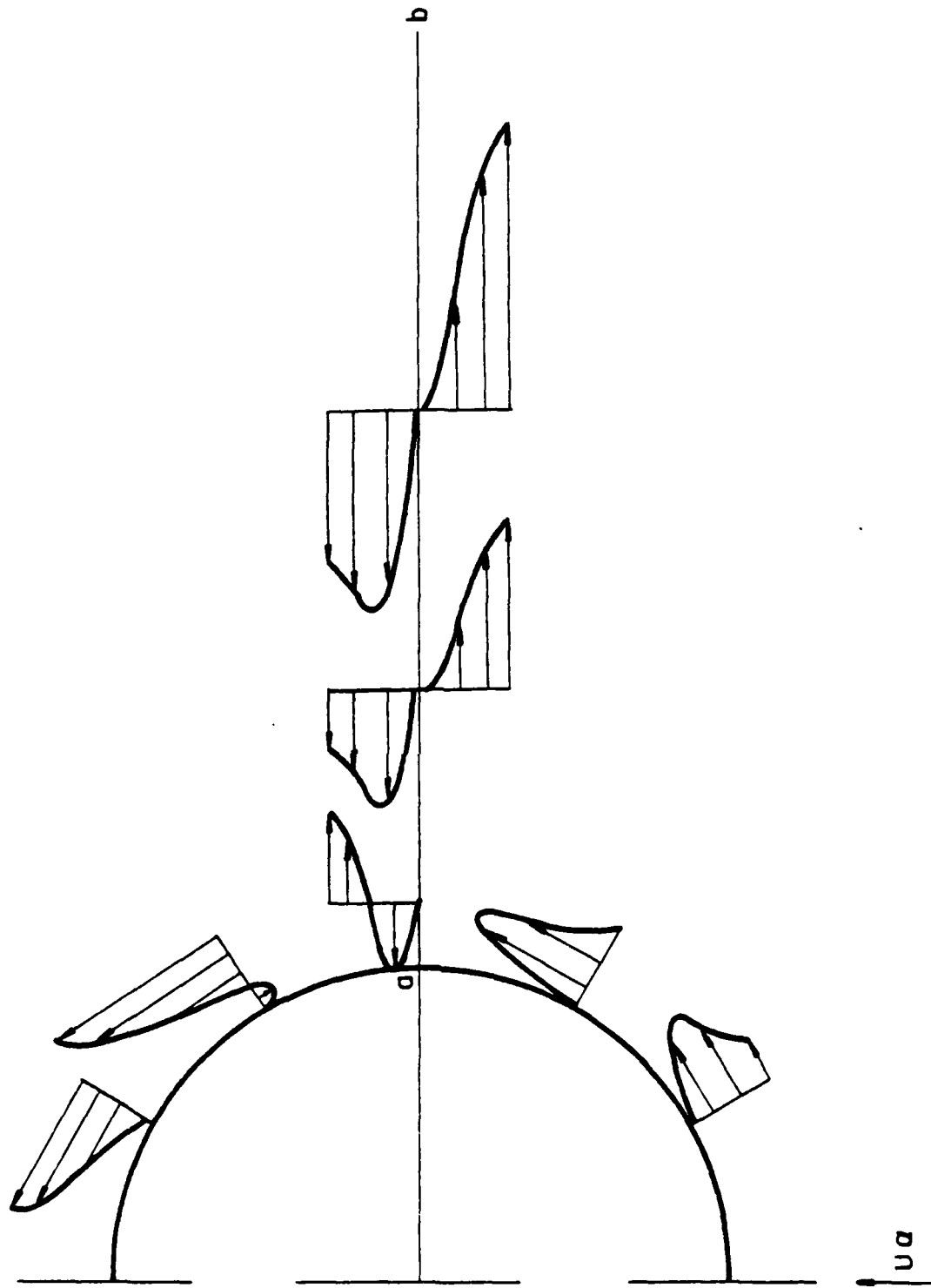


FIG. A11 BOUNDARY LAYER INTERACTION:
 $W-CB, a = 2R_s^{-1/2}, a/b = 0.25$

DATE
FILMED
— 8